NAVAL POSTGRADUATE SCHOOL
Monterey, California

THESIS

PRODUCTION OF ULTRA-FINE GRAINS AND EVOLUTION OF GRAIN BOUNDARIES DURING SEVERE PLASTIC DEFORMATION OF ALUMINUM AND ITS ALLOYS

by

Douglas Lee Swisher

December 2000

Thesis Advisor: Terry McNelley

Approved for public release; distribution is unlimited

REPORT DOCUMENTATION PAGE	*Form Approved OMB No. 0704-0188*

Public reporting burden for this collection of information is estimated to average 1 hour per response, including the time for reviewing instruction, searching existing data sources, gathering and maintaining the data needed, and completing and reviewing the collection of information. Send comments regarding this burden estimate or any other aspect of this collection of information, including suggestions for reducing this burden, to Washington headquarters Services, Directorate for Information Operations and Reports, 1215 Jefferson Davis Highway, Suite 1204, Arlington, VA 22202-4302, and to the Office of Management and Budget, Paperwork Reduction Project (0704-0188) Washington DC 20503.

1. AGENCY USE ONLY *(Leave blank)*	2. REPORT DATE December 2000	3. REPORT TYPE AND DATES COVERED Master's Thesis	
4. TITLE AND SUBTITLE: Title (Mix case letters) roduction of Ultra-Fine Grains and Evolution of Grain Boundaries During evere Plastic Deformation of Aluminum and Its Alloys		**5. FUNDING NUMBERS**	
6. AUTHOR(S) Swisher, Douglas L.			

7. PERFORMING ORGANIZATION NAME(S) AND ADDRESS(ES)
   Naval Postgraduate School
   Monterey, CA 93943-5000
		. PERFORMING ORGANIZATION EPORT NUMBER	

9. SPONSORING / MONITORING AGENCY NAME(S) AND ADDRESS(ES) N/A		**10. SPONSORING / MONITORING AGENCY REPORT NUMBER**	

11. SUPPLEMENTARY NOTES The views expressed in this thesis are those of the author and do not reflect the official policy or position of the Department of Defense or the U.S. Government.

12a. DISTRIBUTION / AVAILABILITY STATEMENT Approved for public release; distribution unlimited.	12b. DISTRIBUTION CODE

13. ABSTRACT *(maximum 200 words)*

Equal channel-angular pressing (ECAP) is a recently developed method for deformation processing of material that can produce an ultra-fine grain structure in bulk material through severe plastic deformation. This study will present results on microstructural evolution during repetitive ECAP of pure aluminum. The principal method of data collection was Orientation Imaging Microscopy (OIM). The results of the study indicate that, after one ECAP pass, the structure is inhomogeneous and anisotropic, and consists mostly of deformation-induced features. After repetitive ECAP, the aluminum material exhibited a homogeneous grain size but retained an anisotropic character to the microstructure. After twelve ECAP passes the microstructure consisted mainly of fine grains surrounded by high-angle boundaries but an appreciable fraction of low-angle boundaries remained. This microstructure thus comprises a mixture of deformation-induced and recrystallization features. Further results were also obtained documenting the existence of deformation banding in this material as well as in a rolled aluminum alloy. This phenomenon may be general in nature and associated with severe plastic deformation in aluminum and its alloys.

14. SUBJECT TERMS Equal Channel-Angular Pressing, Ultra-fine Grains, Grain Refinement, Plastic Deformation, Deformation Banding, Misorientation Angle, Orientation Imaging Microscopy, Electron Backscatter Diffraction, Supral 2004, Nano Structures, Severe Plastic Deformation	15. NUMBER OF PAGES 86
	16. PRICE CODE

17. SECURITY CLASSIFICATION OF REPORT Unclassified	18. SECURITY CLASSIFICATION OF THIS PAGE Unclassified	19. SECURITY CLASSIFICATION OF ABSTRACT Unclassified	20. LIMITATION OF ABSTRACT UL

NSN 7540-01-280-5500

Standard Form 298 (Rev. 2-89)
Prescribed by ANSI Std. 239-18

i

THIS PAGE INTENTIONALLY LEFT BLANK

PRODUCTION OF ULTRA-FINE GRAINS AND EVOLUTION OF GRAIN BOUNDARIES DURING SEVERE PLASTIC DEFORMATION OF ALUMINUM AND ITS ALLOYS

Douglas Lee Swisher
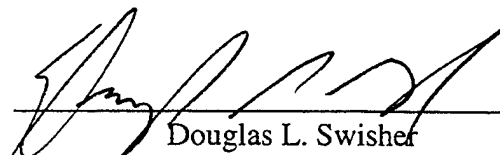Lieutenant, United States Navy
B.S., United States Naval Academy

Submitted in partial fulfillment of the
requirements for the degrees of

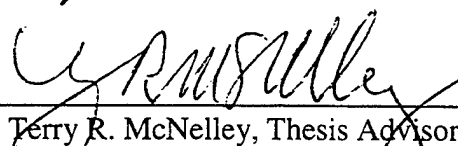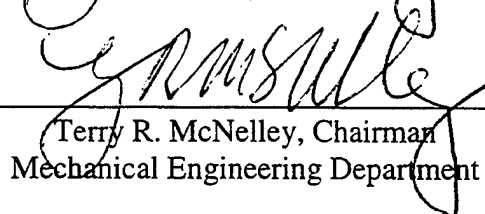## MECHANICAL ENGINEER and MASTER OF SCIENCE IN MATERIALS SCIENCE AND ENGINEERING

from the

NAVAL POSTGRADUATE SCHOOL
December 2000

Author: _____
Douglas L. Swisher

Approved by: _____
Terry R. McNelley, Thesis Advisor

_____
Terry R. McNelley, Chairman
Mechanical Engineering Department

THIS PAGE INTENTIONALLY LEFT BLANK

ABSTRACT

Equal channel-angular pressing (ECAP) is a recently developed method for deformation processing of material that can produce an ultra-fine grain structure in bulk material through severe plastic deformation. This study will present results on microstructural evolution during repetitive ECAP of pure aluminum. The principal method of data collection was Orientation Imaging Microscopy (OIM). The results of the study indicate that, after one ECAP pass, the structure is inhomogeneous and anisotropic, and consists mostly of deformation-induced features. After repetitive ECAP, the aluminum material exhibited a homogeneous grain size but retained an anisotropic character to the microstructure. After twelve ECAP passes the microstructure consisted mainly of fine grains surrounded by high-angle boundaries but an appreciable fraction of low-angle boundaries remained. This microstructure thus comprises a mixture of deformation-induced and recrystallization features. Further results were also obtained documenting the existence of deformation banding in this material as well as in a rolled aluminum alloy. This phenomenon may be general in nature and associated with severe plastic deformation in aluminum and its alloys.

THIS PAGE INTENTIONALLY LEFT BLANK

TABLE OF CONTENTS

THIS PAGE INTENTIONALLY LEFT BLANK

ACKNOWLEDGMENTS

THIS PAGE INTENTIONALLY LEFT BLANK

I.   INTRODUCTION

A.   DEFORMATION PROCESSING AND GRAIN REFINEMENT

Throughout recorded history the ability of metals to sustain plastic deformation has been put to use in the shaping of metallic materials and production of useful implements. It has also been understood that plastic deformation strengthens metals, and that incorporating annealing treatments to soften the material during shaping processes may afford further control of both the process and the resulting material properties. For most of this history the mechanisms involved during deformation and annealing have not been known and understanding of these processes has been entirely empirical. The application of various microscopy techniques and X-ray diffraction methods [Refs. 1, 2] to the study of microstructure in metallic materials has revealed the polycrystalline nature of metallic materials. Deformation at low temperature results in distortion of the grain structure as dislocations are generated, move and become immobilized. This constitutes strain hardening and results in energy storage in the form of dislocation arrays. Annealing may result in recovery, i.e., softening associated with dislocation rearrangement, or in the formation and growth of new, strain free grains, i.e. recrystallization, within the microstructure [Ref. 3]. Thus, deformation and annealing treatments may allow control of the grain structure and grain size of metals.

Grain size is an important factor in the mechanical properties of materials. Generally, refinement of the grain size results in improvements in both strength and toughness of metals [Refs. 4, 5]. In alloys of metals such as iron and titanium the phase transformations that occur during cooling provide a significant degree of grain size control. In many other metals, such as aluminum, nickel and copper, grain size

1

refinement in wrought alloys may only be achieved by deformation and recrystallization, although our understanding of these mechanisms during industrial processing is still largely empirical [Refs. 6, 7]. As recently as 1993 Haasen [Ref. 8] has observed that recrystallization is the last major unexplored frontier in physical metallurgy.

Grain sizes in the range of ~20 - 50 μm are typical of engineering alloys commonly produced today. However recent research has demonstrated that grains can be readily refined to 1.0 μm in size and still finer grain sizes of perhaps 100 nm or less can also be achieved [Refs. 9, 10]. Such ultra-fine grained materials may exhibit dramatic improvements in the previously mentioned mechanical properties and many potential applications exist for the increased mechanical properties afforded by these materials. Applications include those requiring an increased strength to weight ratio, resistance to cyclic loads or those requiring increased fracture toughness.

B. PRODUCTION OF ULTRA-FINE GRAINS IN METALS

Ultra-fine grain size has been achieved during powder processing [Refs. 9, 10] or in association with various deposition processes. However, the quantity of material produced by such methods is limited and the costs are often prohibitive. In bulk materials, methods of grain size refinement of alloys have included thermal treatments in conjunction with phase transformations, when available, and with deformation processing. Recent studies have shown that ultra-fine grain sizes in the submicrometer or even nanometer range can be achieved by plastic deformation involving extremely large plastic strains [Refs. 11-14]. A potential limitation in many deformation processing operations is that the necessary shape change associated with many of the processes may limit the starting and ending sizes and shapes of the material.

A new method of producing a severely deformed material with no change in cross-sectional area has recently been developed [Refs. 11-14]. This process, which is called Equal Channel-Angular Pressing (ECAP), consists of pressing a billet of material through a die having two channels, of equal cross section, that intersect at an angle. The billet experiences simple shear without change in cross-sectional area upon passage through the intersection of the die channels and so the process is amenable to repetition. Extensive investigations of microstructural evolution during ECAP of pure aluminum and selected aluminum alloys have been reported by Langdon and coworkers [Refs. 14-24]. Transmission electron microscopy results have indicated that the grain size of pure aluminum may be refined to about 1.2 μm during ECAP at room temperature and that grain sizes of ≈ 200 nm may be attained during room temperature ECAP of selected alloys. In this work, assessment of grain size refinement relied on selected area electron diffraction (SAED) methods in transmission electron microscopy (TEM) [Refs. 17, 19].

3

The lattice orientation differences, or disorientations, of grain boundaries in a polycrystalline material must be predominantly high-angle in nature to meet the requirements for a fine grain structure. Since deformation processing may also introduce fine subgrains of low disorientation it is necessary to determine grain-to-grain disorientations as well as the apparent grain size. The use of SAED in TEM may not provide an unambiguous assessment of the nature of grain boundaries and thus the state of the microstructure. Recently developed computer-aided electron backscatter diffraction (EBSD) analysis methods using a scanning electron microscope (SEM) are now available to obtain statistically significant grain-to-grain disorientation data as well as grain size values [Ref 25]. Further background on ECAP will be provided in the following chapter. Its microstructural effect on pure aluminum will then be characterized via EBSD methods with particular attention to refinement of the grain size and to characterization of the nature of the grain boundaries resulting from this method of processing.

II. BACKGROUND

A. EQUAL CHANNEL-ANGULAR PRESSING

Initial development of ECAP as a practical method of deformation processing took place in Russia and was conducted by Valiev and his coworkers [Refs. 11, 12]. Extremely large cumulative plastic strains may be induced in a material due to the repeatability of the process. A simplified schematic of an ECAP apparatus is presented in Figure 2.1 (a). In this case the angle between the die channels, ϕ, is 90°; all material examined in this study was pressed through such an ECAP die. The die design also includes a relief angle, ψ, which is 20° for the die channel of this work. The relief angle along the outer radius of the die channel is required in order to minimize the friction effects and allow the billet to pass through the die.

During an ECAP pass a cylindrical billet is pressed downward through the vertical die channel as indicated in Figure 2.1(a). As the billet passes through the channel intersection, a shearing of the billet takes place. Figure 2.1 (b) shows an actual billet of 99.99% pure aluminum after ECAP processing.

A simplified two-dimensional schematic illustration in Figure 2.2 shows an element ABCD, which lays in the y plane, before pressing and the same element, A'B'C'D', after passage through the die channel intersection. The accumulated Von Mises equivalent strain that accompanies N pressing passes through such an ECAP die may be calculated as seen in Equation 2.1 [Ref. 20].

$$\varepsilon_N = \left(\frac{N}{3^{1/2}}\right)\left[2\cot\left(\frac{\phi}{2}+\frac{\psi}{2}\right)+\psi\cos ec\left(\frac{\phi}{2}+\frac{\psi}{2}\right)\right] \qquad \text{Equation 2.1}$$

For a 90° die angle and 20° relief angle $\varepsilon_N = 1.055N$, i.e. the Von Mises equivalent strain is 1.055 for each pressing pass.

As noted earlier, there is no reduction in cross-sectional area during a pressing pass and so this is a repeatable process. The four distinct routes that have been commonly employed in repetitive ECAP are depicted in Figure 2.3 [Ref. 19]. These are defined as follows: Route A involves no rotation of the sample between successive pressing operations; in Route B_A, the sample is rotated 90° between successive pressings in an alternating sense (i.e. clockwise 90°, then counter-clockwise 90°, then clockwise 90°, etc.); Route B_C also involves rotation by 90° after each pressing operation but the rotational direction is constant (i.e., always clockwise or counter-clockwise); finally Route C involves a 180° rotation after each pass through the ECAP die.
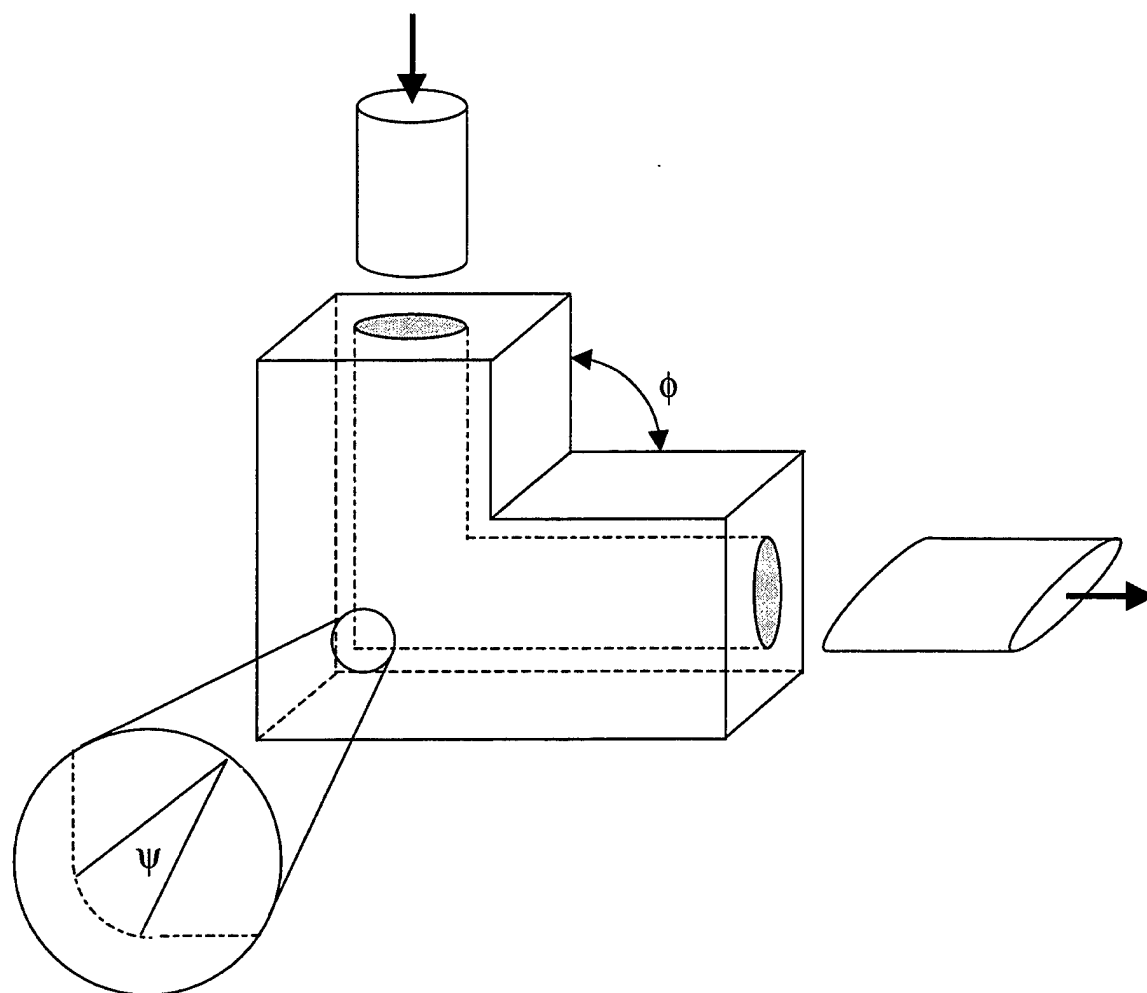
(a)
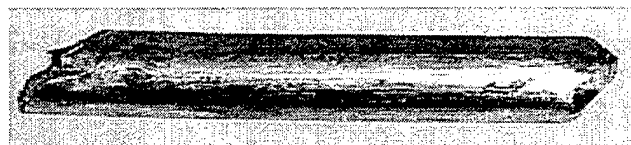
(b)

Figure 2.1. A schematic representation of an Equal Channel-Angular Pressing (ECAP) die. The angle between die channels is $\phi=90°$; the shearing of a cylindrical billet during pressing is shown and the angles ϕ and ψ, which is the relief angle at the outer radius of the channel intersection, are defined; (b) shows a sample after pressing.
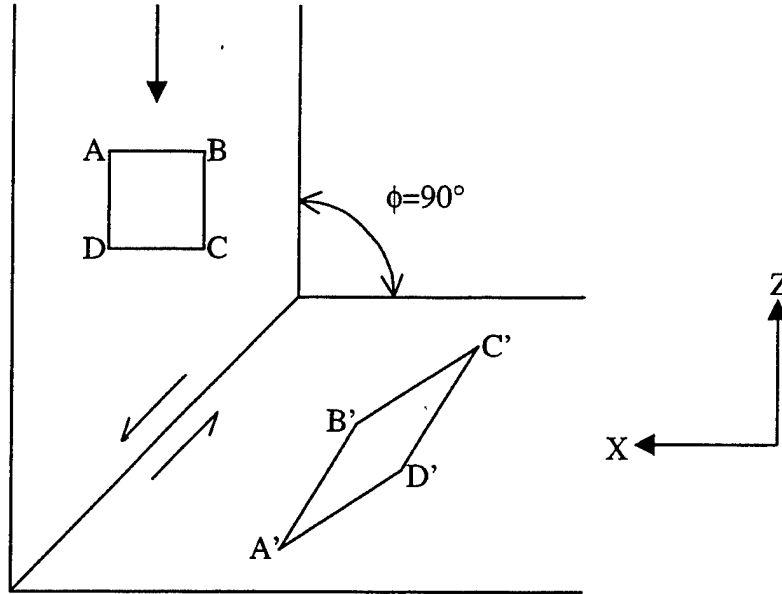
Figure 2.2. Schematic of the shearing process. As a volume element ABCD passes through the shear plane, it is sheared to the shape A'B'C'D'; for a die angle ϕ=90°, the von Mises equivalent strain ε_N = 1.055.
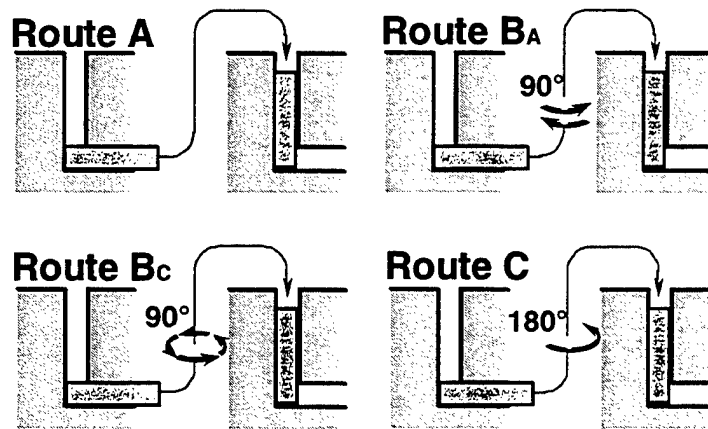

Figure 2.3. Schematic of four different Equal Channel-Angular Pressing routes for repetitive pressings. Route A involves no rotation between passes, Route B_A involves alternating 90° rotations, Route B_C has rotations of 90° in the same sense while Route C has rotations of 180° between successive passes. [From Ref. 19].

B.   EVALUATION OF GRAIN REFINEMENT

A grain in a polycrystalline pure metal is a region of constant lattice orientation. The lattice orientation changes at the boundary between adjacent grains; this change in orientation typically occurs over two or three atom distances at such boundaries. Thus, the orientation difference, or disorientation, between adjacent grains is a characteristic feature in addition to the grain size that may be employed to describe a grain structure. Figure 2.4 is a schematic representation of two adjacent grains and the orientation of the cubic lattice within each grain. Boundaries of small disorientation angle ($\theta \leq 5°$) are often the result of plastic deformation and may be thought of as arrays of dislocations so that there is a high degree of lattice registry across the boundary plane [Ref. 26].

Boundaries must be effective barriers to the motion of lattice dislocations in order to contribute to strengthening, e.g. as envisioned in the Hall-Petch [Refs. 4, 5] model for grain size strengthening. Small angle boundaries would be relatively ineffective due to lattice registry across the boundary, and so the characterization of grain-to-grain disorientations is as important as determination of grain size. This can be accomplished using EBSD methods.

In the simplest terms, the disorientation angle is the lowest degree of rotation about an associated rotation axis that will bring the lattice of one grain into coincidence with the lattice of the other grain. Figure 2.5 is a schematic illustration of two cubic lattices that are disoriented by rotation through an angle ϕ about the Z-axis. As also noted, the disorientation angle could also be taken as $\pi/2 - \phi$, $\pi - \phi$, or $3\pi/2 - \phi$ due to crystal symmetry. Thus, in general there are multiple, crystallographically equivalent rotations that will bring the lattices into coincidence. In a cubic system there can be up to

24 possible rotations and associated rotation axes that would result in bringing two lattices into coincidence. By convention, the disorientation angle is taken to be the minimum absolute rotation angle between two adjacent lattices.

A reference axis system is needed in order to determine grain-to-grain disorientations. In studies of deformed materials the reference axes are usually chosen to reflect the deformation process. Because rolling is perhaps the most important deformation processing method the reference axis system is taken by convention to be x_1 ∥ to the rolling direction (RD), x_2 ∥ to the transverse direction (TD), and x_3 ∥ to the sheet normal direction (ND) [Ref. 25]. Then, the orientation of the cubic lattice is represented by a set of three Euler angles, ϕ_1, Φ and ϕ_2, that reorient the cubic lattice from the reference axis system into the observed lattice orientation in the material. The Euler angles are defined according to Bunge's convention [Refs. 25, 27]. This convention states that ϕ_1 is the first rotation and it is about the x_3-axis, Φ is the second rotation and it is about x_1, and ϕ_2 is the final rotation, which is also about x_3 (for ECAP processing, x_1 is equivalent to the X direction, x_2 the Y direction and x_3 the Z direction). Using this sequence of rotations, any cubic lattice orientation can be described with respect to the reference axis system.

The Euler angles for the cubic lattice of a given grain may be used to obtain an orientation matrix, [A], as in Equation 2.2. If a similar orientation matrix is obtained for an adjacent grain the disorientation matrix, [M], may then be computed using Equation 2.3. In practice there are, again, up to 24 possible disorientation matrices and so determination of the disorientation angle, θ, involves a minimization operation among the crystallographically equivalent disorientation matrices. The disorientation angle, θ, is

10

then found from Equation 2.4, where m_{11}, m_{22} and m_{33} are the diagonal terms of the [M]

having the lowest rotation angle. The range of θ for a cubic system is $0°$ to $62.8°$ due to

the symmetry.

$$[A_1] = \begin{bmatrix} \cos\phi_1\cos\phi_2 - \sin\phi_1\sin\phi_2\cos\Phi & \sin\phi_1\cos\phi_2 + \cos\phi_1\sin\phi_2\cos\Phi & \sin\phi_2\sin\Phi \\ -\cos\phi_1\sin\phi_2 - \sin\phi_1\cos\phi_2\cos\Phi & -\sin\phi_1\sin\phi_2 + \cos\phi_1\cos\phi_2\cos\Phi & \cos\phi_2\sin\Phi \\ \sin\phi_1\sin\Phi & -\cos\phi_1\sin\Phi & \cos\Phi \end{bmatrix}$$ Equation 2.2

$$[M] = [A_1]^{-1}[A_2]$$ Equation 2.3

$$\theta_{12} = \min\left|\arccos\left[\frac{1}{2}\left(m_{11}^{12} + m_{22}^{12} + m_{33}^{12} - 1\right)\right]\right|$$ Equation 2.4
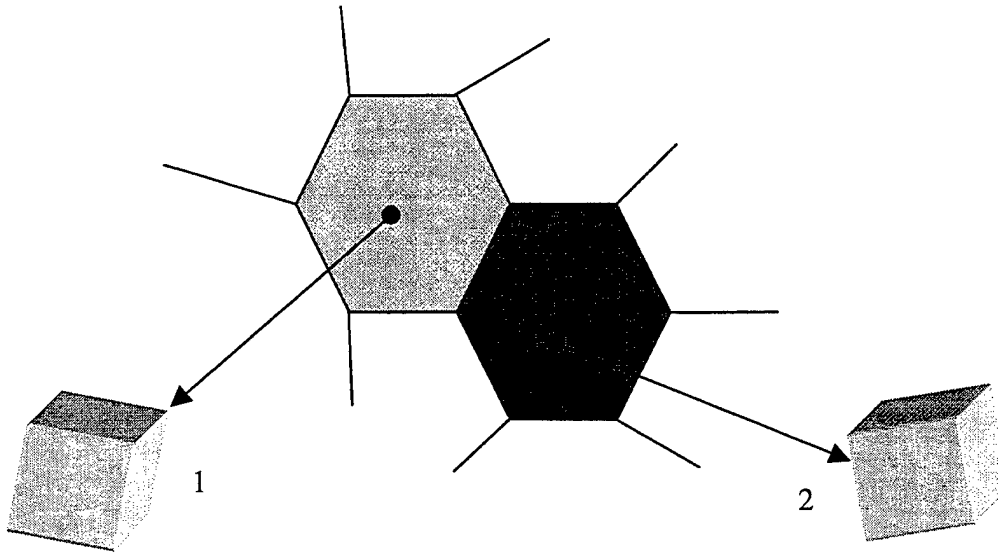

Figure 2.4. Schematic of two adjacent grains and the orientation of the cubic lattice within each grain.

11
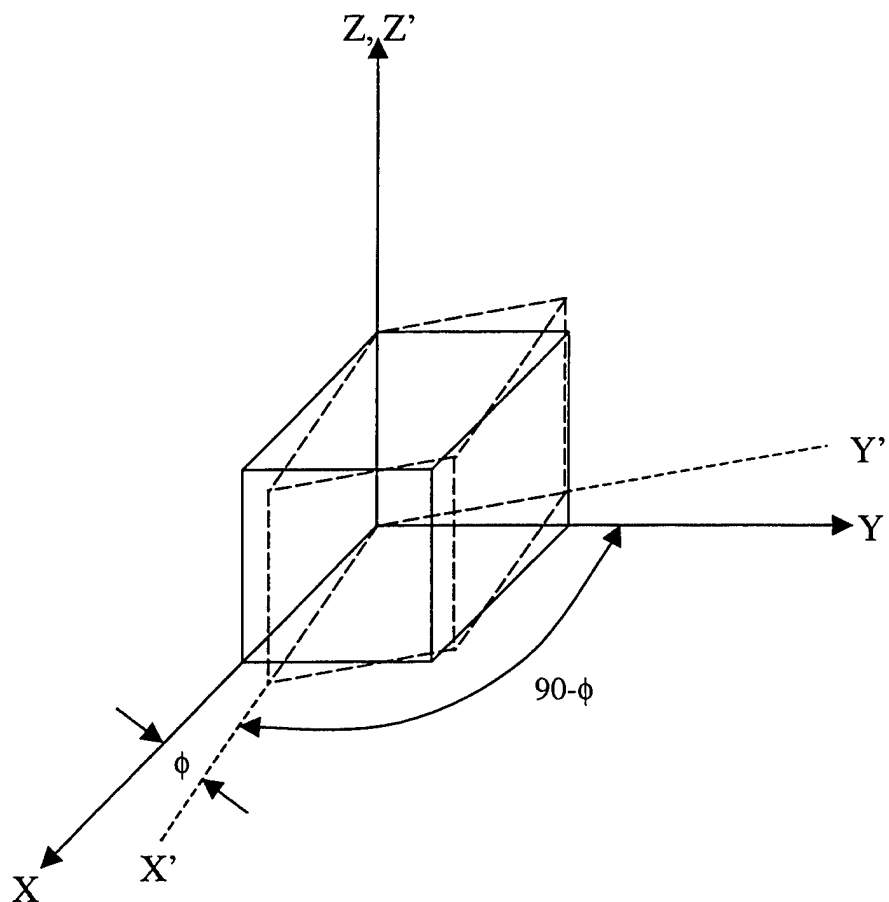
Figure 2.5. Example of two cubes misoriented by a rotation about Z. A rotation of either ϕ or $90°$-ϕ about the Z-axis will bring the cubes into coincidence; by convention, the disorientation is taken as the minimum angle, which is ϕ.

C.   OBJECTIVES OF THIS RESEARCH

The main objective of this research was to characterize the microstructural evolution in pure aluminum (99.99%) during repetitive pressing operations by ECAP. This was accomplished mainly by use of computer-aided EBSD methods and orientation imaging microscopy (OIM) techniques which allow direct measurement of grain-specific lattice orientations and thus quantitative assessment of grain-to-grain disorientations. The OIM approach allows determination of grain size in terms of regions of common lattice orientation and thereby also allows determination of grain boundary disorientations in relation to the extent of ECAP processing. Altogether, such characterization may allow determination of the degree of recrystallization attained via ECAP. During the course of this work the occurrence of the phenomenon of deformation banding was noted, both in aluminum processed by ECAP and in an aluminum alloy that had been processed by rolling. A secondary objective of this work was to document this phenomenon in aluminum.

THIS PAGE INTENTIONALLY LEFT BLANK

III. EXPERIMENTAL PROCEDURES

A. ECAP PROCESSING

The material examined in this research were provided by Langdon and coworkers and details of the material and processing have been given previously [Ref. 17]. Commercially pure (99.99%) aluminum ingot was processed to the form of a bar 10 mm in diameter and which was then annealed to provide an initial grain size ≈ 1.0 mm prior to ECAP. The die channel was of circular cross section with a diameter of 10 mm, 90° angle between the die channels, and with a 20° arc at the outer radius of the channel intersection. The bars were cut into billets 60 mm in length. ECAP was conducted at room temperature (25°C) by placing a billet in the vertical die channel and then pressing it through the die with a plunger. Adiabatic heating during pressing at 19 mm s^{-1} resulted in a temperature rise to about 40°C over an interval of about 1 s as the material passed through the intersection of the die channels; thereafter the billet cooled to room temperature in about 60 s after pressing. Material was examined after one pressing pass, and after repetitive pressing via route B_C for either 4 or 12 pressing passes.

B.   SAMPLE PREPARATION FOR EBSD EXAMINATION

Samples were sectioned from as-pressed billets using a Buehler low-speed saw with a diamond-wafering blade. With reference to the axes defined in Figure 3.1, a disc of 2 mm thickness and with the X direction as its normal was sectioned from the as-pressed cylindrical billet. These axes are always defined in reference to the final pressing pass for materials from billets that have been subjected to repetitive pressing operations. A second cylindrical section ~10 mm in length was cut and then reoriented in order to section and provide a plane that contained the center line of the billet and whose normal is the Y direction.

Mechanical polishing of the samples was accomplished by carrying out the steps outlined in Table 3.1 for the indicated times. The silicon carbide (SiC) paper was used on a flat surface with water as the lubricant, and grinding was conducted in one direction until all evidence of the prior grinding step was eliminated. The sample was then rotated 90° and the process was repeated. Rotating wheels were used for polishing, which was carried out in three stages. Care was exercised to employ dilute diamond abrasive suspensions and a dilute colloidal silica suspension to avoid surface contamination with these abrasives. After each mechanical polishing step, an ultrasonic cleaning was performed for 10 minutes in ethanol.

A distortion-free final polish was required due to the very small interaction volume near the surface of the sample associated with formation of the diffraction patterns by the electrons. Hence, the final polishing step was an electropolish conducted in a Buehler Electromet 4 apparatus using a 20% Perchloric Acid - 80% Ethanol

electrolyte solution that was cooled to -25°C. Samples were examined in the as polished condition.

Step	Abrasive	Time	RPM
1	500 Grit SiC Paper	30 sec.	n/a
2	1000 Grit SiC Paper	30 sec.	n/a
3	2400 Grit Sic Paper	30 sec.	n/a
4	4000 Grit SiC Paper	30 sec.	n/a
5	3 μm Metadi Diamond Suspension	10 min.	180
6	1 μm Metadi Diamond Suspension	10 min.	180
7	0.05 μm Colloidal Silica	10 min.	120

Table 3.1. Mechanical Polishing

The relationship of the sample surfaces that are to be examined to the as-pressed billet is depicted in Figure 3.2. It is important to note that care must be taken to identify the positive senses of the X, Y and Z axes due to the low symmetry associated with ECAP which is a process involving pure shear. For example, the X – Z plane is not a mirror plane and if the sense of the Y direction is not correctly determined the resulting data may suggest a shear direction rotated 90 ° from its expected orientation.
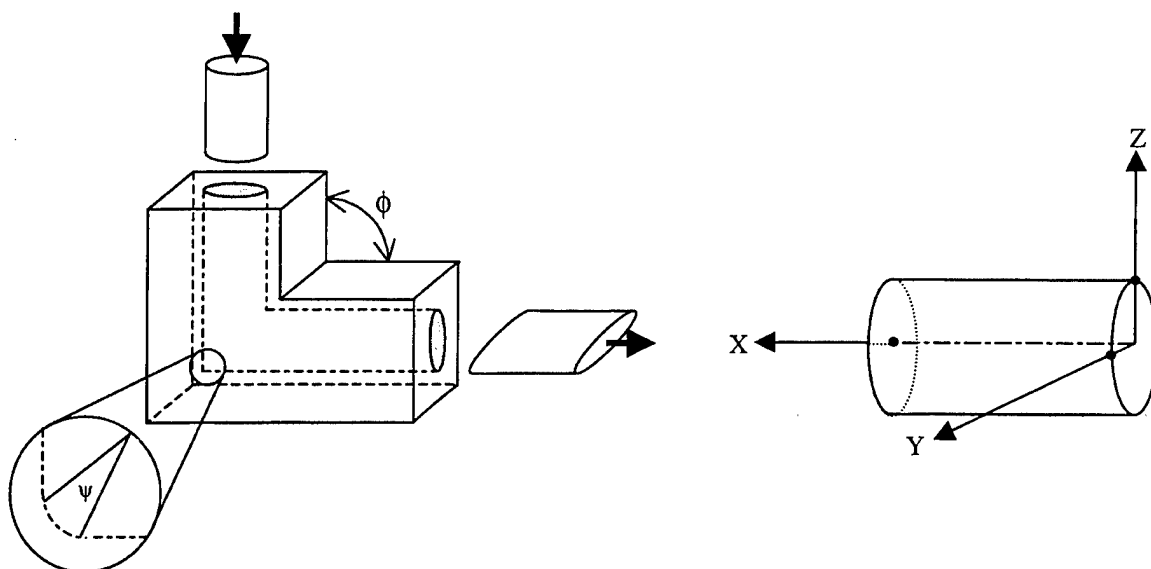
Figure 3.1. The reference axis system associated with the Equal Channel-Angular Pressing apparatus. The positive X direction has been taken as being directed *toward* the ECAP apparatus.
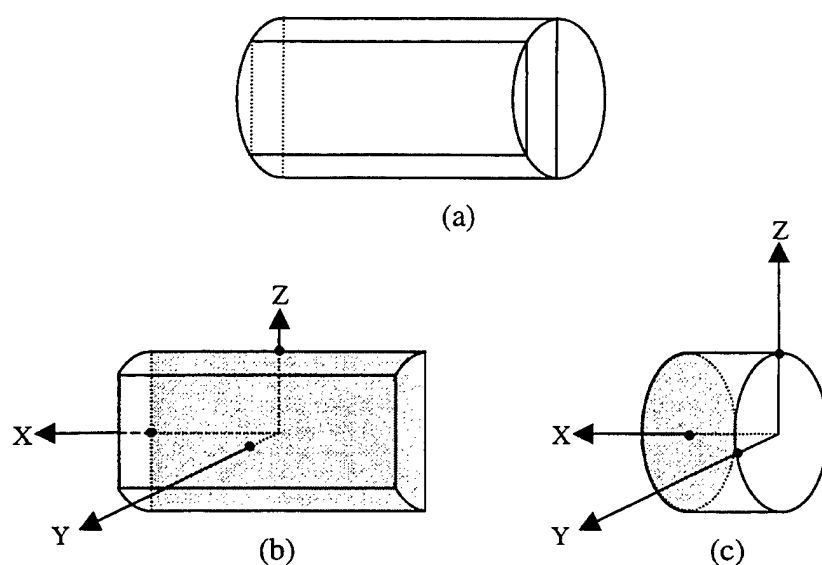

(a)

(b)

(c)

Figure 3.2. Schematic showing the sectioning of samples for EBSD analysis. In (a), the approximate shape of the samples after sectioning is illustrated for (b), the Y plane and (c), the X Plane. The shaded regions indicate the actual surface examined.

C.   ELECTRON   BACKSCATTER   PATTERN   COLLECTION   AND ANALYSIS

A TOPCON SM-510 Scanning Electron Microscope (SEM) with a tungsten filament was used for data collection and analysis. The microscope was operated at an accelerating voltage of 20kV. After polishing, the samples were put into the SEM in a holder that inclines the sample surface at 70° to the vertical. This was done in order to utilize the EBSP analysis capability of the Orientation Imaging Microscopy (OIM) hardware and software provided by TexSEM, Inc. The orientation of the sample in the SEM chamber is illustrated schematically in Figure 3.3(a) while Figures 3.3(b) and (c) represent the orientation of the sample as viewed from the camera position.

The fixed reference axes assigned in software and from which the Euler angles were calculated are defined as follows: the RD direction is assigned as positive downward; ND is positive toward the phosphor screen; and TD is parallel to the horizontal.

The SEM was operated in spot mode with an electron beam diameter of about 0.15 µm. The electrons interact within the first 30 - 50 nm of the sample surface, undergoing Bragg diffraction and thereby providing orientation information from a region as small as 0.15 µm in diameter. The diffracted electrons impinge upon a phosphor screen, thus illuminating it. A low-light level camera captured the image of the diffraction pattern on the phosphor screen and the OIM software analyzed the pattern to determine the corresponding lattice orientation. Figure 3.4 shows a representative Kikuchi pattern before and after indexing, the associated pole figure and corresponding lattice orientation.

In practice, each pattern is analyzed several times, and resulting solutions, in the form of the Euler angles ϕ_1, Φ, and ϕ_2 are then ranked in the software. The pattern is then assigned a best-fit solution and an indication of the goodness of the solution which is called the Confidence Index (CI). CI values greater than 0.1 correspond to a 95% probability correct indexing. The pattern index was then saved in the following format: the Euler angles ϕ_1, Φ, and ϕ_2, the coordinate location on the sample surface for the pattern, and the assigned CI value. OIM is accomplished by progressively displacing the electron beam over a preselected area on the sample surface in a raster pattern. The local lattice orientation at each successive beam position in the raster pattern is obtained as described above. The resulting data file may then be employed to construct an image based on these orientation measurements. Typical scans were conducted over areas of 20 μm x 20 μm using a step size between successive measurements of 0.2μm. Runs over areas 100 μm x 100 μm in size, using 1.0 μm step sizes, were also employed. Current OIM systems can obtain and index patterns at the rate of about three every second, or about 10,000 per hour.

One problem area encountered had to do with obtaining diffraction patterns occurred when the crystal lattice had curvature present due to a sufficiently high dislocation density. This would be indicated by the absence of patterns on the television monitor, e.g. as seen in Figure 3.5(a). A second common problem encountered was the electron beam being incident on a grain boundary so that both crystal lattice orientations provided diffracted electrons thus overlapping patterns were produced on the viewing screen; an example may be seen in Figure 3.5(b).

20

Data clean up procedures to alleviate such problems are included in software and were performed in two successive steps. First, in effect the highest CI for a grain would be assigned to all points in that grain. Second, a data point (orientation) with a CI less than 0.1 would be compared to its nearest neighbors and the orientation of the neighbor with the highest CI would be assigned to the point, thus effectively incorporating it within a grain. This clean up step assumed that the low CI points are occurring near grain boundaries, or areas of high dislocation density and that the point with the higher CI is the true orientation.

It should be noted that any single orientation with a CI value greater than 0.1 will not be altered. Grains with good quality EBSP's, no matter what size, will be kept. The elimination of low CI points is done in order to obtain a higher fidelity picture of the grain boundary regions and thus a more accurate determination of the disorientation angle between grains. Accepted accuracy of individual grain orientations in OIM is 1° or better; on this basis, the resolution of grain-to-grain disorientations here is taken to be 2°.

After the clean up procedure was completed, the OIM software allowed the production of OIM grain maps, pole figures representing the texture, rotation angle histograms, and various other representations of the data. Grain maps are typically color coded maps where a common color is assigned to contiguous points of common orientation, i.e. grains. Raw histogram data obtained by OIM are shown in Figure 3.6. Also shown in Figure 3.6 is a representative example of a MATLAB generated seventh order polynomial curve fit to rotation angle data obtained from a series of scans from homogeneous material.
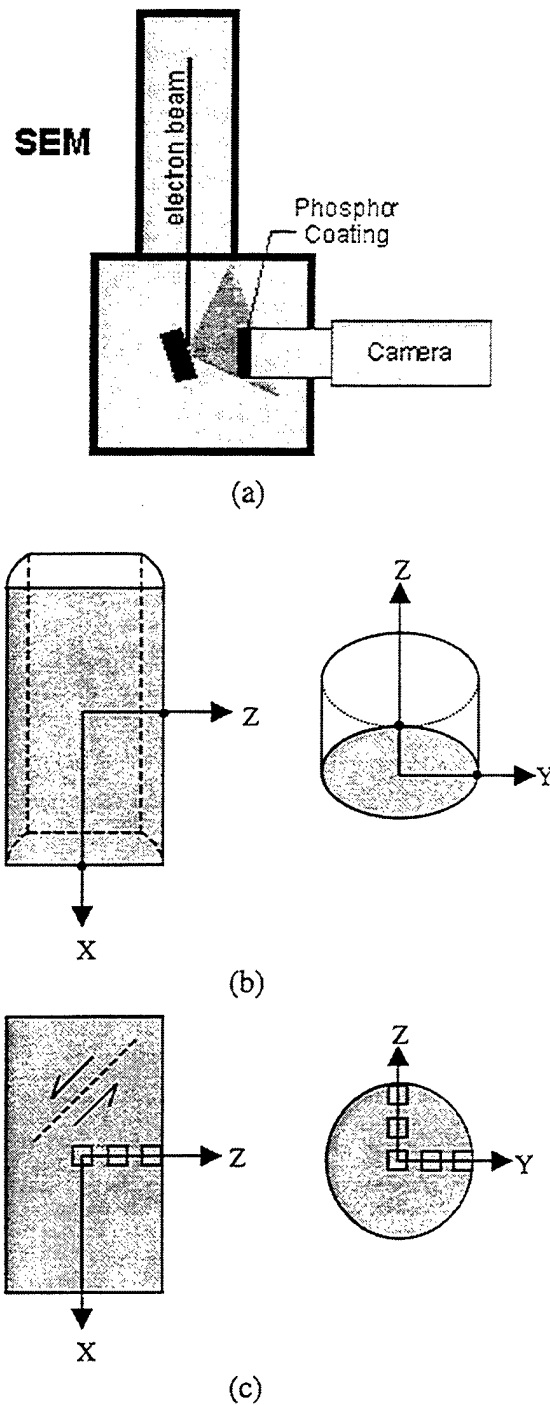
Figure 3.3. Simplified schematic [From Ref. 28] of the Orientation Imaging Microscopy set-up (a), and the sample placement (b), (c) in the microscope: either the Y or X Plane is shown when viewed from the camera position. Simplified, two-dimensional (c) view of the Y and X Planes, indicating the approximate positions where data were collected, namely the sample center, the half or full radius in the Z direction.
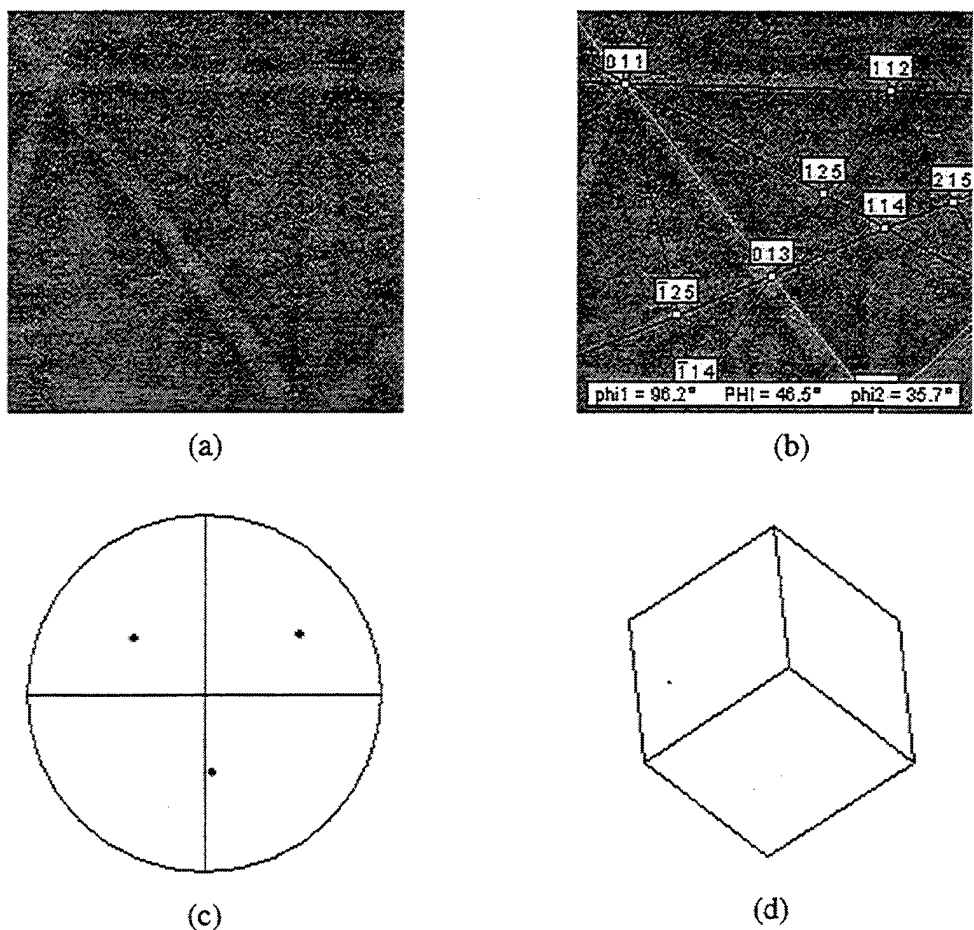
(a)

(b)

(c)

(d)

Figure 3.4. Sample Kikuchi pattern and indexing. In (a), an actual Kikuchi pattern obtained on the video screen is shown; (b), an indexed pattern showing several low-index poles [011], [112], [125], etc.; and Euler angles phi1, PHI and phi2 for this orientation. A pole figure is shown in (c), representing the orientation of the indexed pattern for the <100> poles. Cubic crystal (d) orientation represented by this pattern.
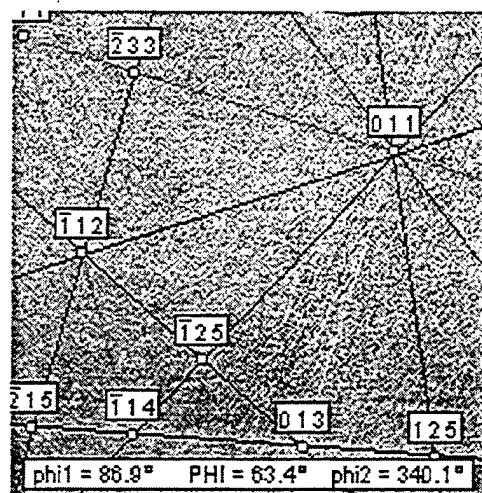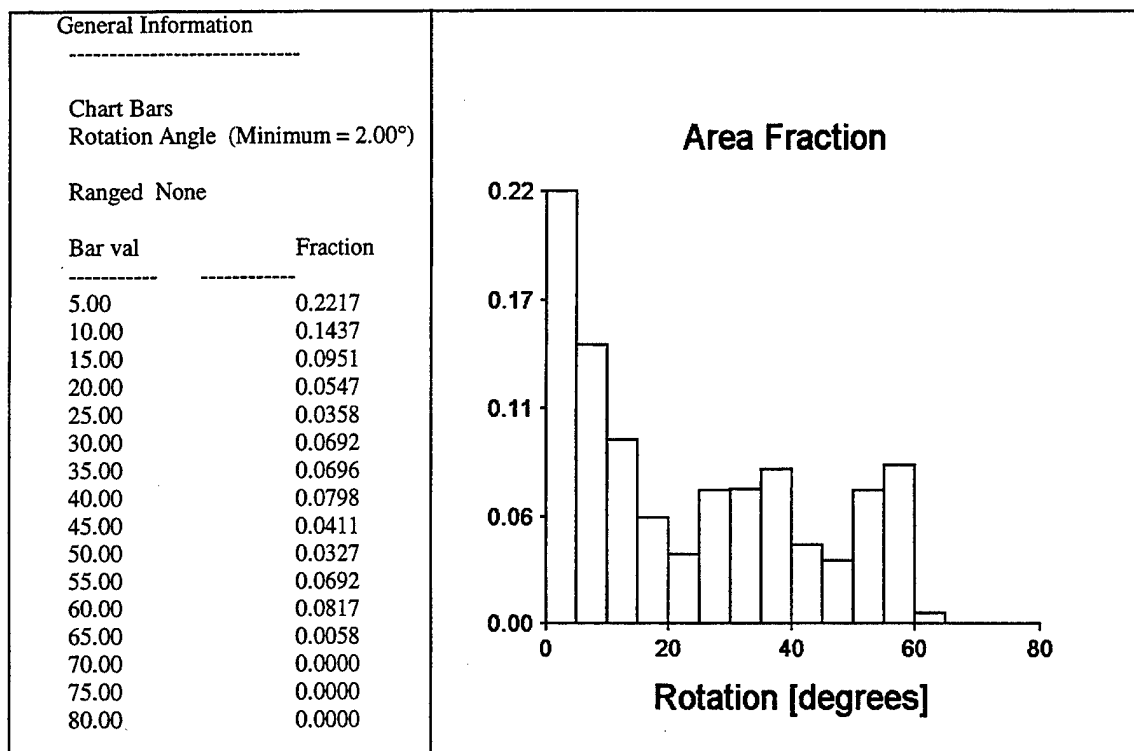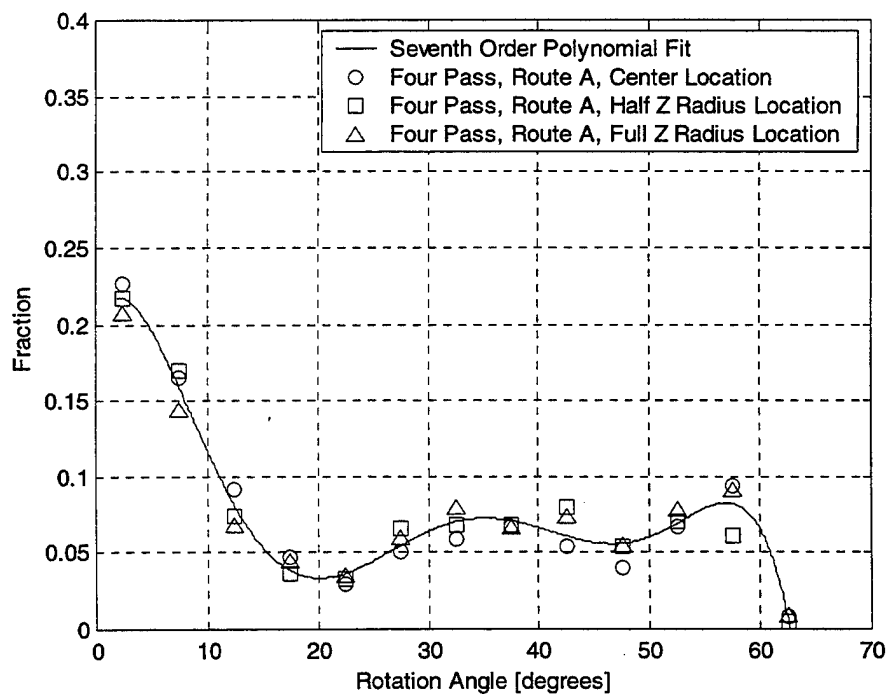
(a)
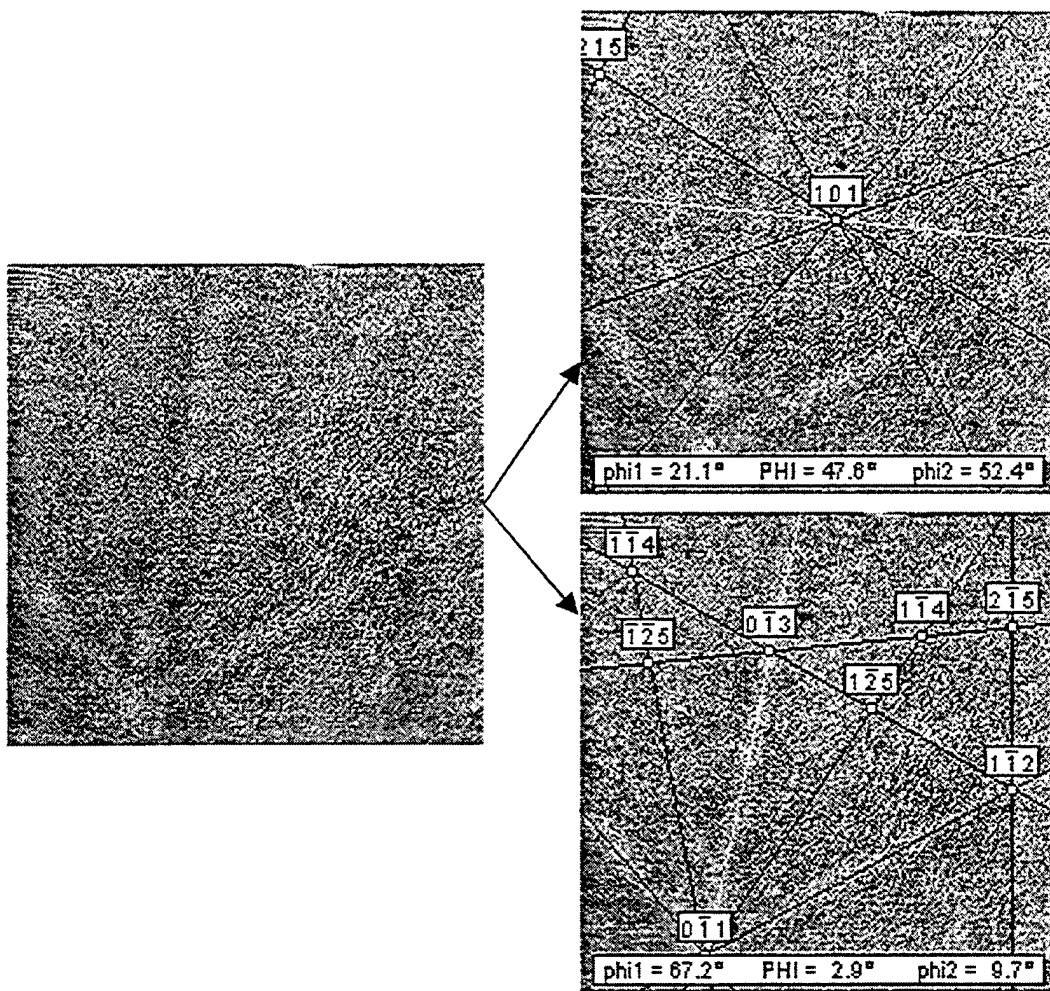
(b)

Figure 3.5. Examples of two common problems encountered when using Electron Back-Scatter Pattern imaging, namely (a) no patterns visible or (b) multiple, overlapping patterns apparent.

24

General Information

Chart Bars
Rotation Angle (Minimum = 2.00°)

Ranged None

Bar val	Fraction
5.00	0.2217
10.00	0.1437
15.00	0.0951
20.00	0.0547
25.00	0.0358
30.00	0.0692
35.00	0.0696
40.00	0.0798
45.00	0.0411
50.00	0.0327
55.00	0.0692
60.00	0.0817
65.00	0.0058
70.00	0.0000
75.00	0.0000
80.00	0.0000

(a)

(b)

Figure 3.6. Representative example of the raw Rotation Angle data obtained from OIM. In (a), a rotation angle histogram from 20μm X 20μm scanned region is shown with a minimum rotation angle set to 2°; (b) Seventh Order Polynomial Least Square fit obtained from six scans for a homogeneous condition of the material.

25

D.   BACKSCATTER ELCECTRON IMAGING

A Cambridge SEM equipped with a LaB_6 filament was used in order to capture the backscatter electron (BSE) images. Secondary electron images were not captured due to the lack of etching on the sample surface (i.e., no surface features were visible). Samples were place in a flat position in the microscope. The accelerating voltage was set to 20 kV and the working distance was reduced to less than 10 mm in order to obtain acceptable orientation contrast in the BSE images of this pure ECAP aluminum.   The BSE images were then captured using SEMICAPS software. This imaging technique was used to provide an independent assessment of the microstructure.   An important limitation of BSE imaging is that grain-to-grain disorientations cannot be determined by this method.

E.   ERROR ANALYSIS

The distribution of the grain-to-grain disorientations, as represented by histograms

of relative number of boundaries as a function of disorientation angle, will be employed

here as a measure of the influence of processing on the grain boundaries in this material.

It is therefore important to know the errors associated with such measurements. There are

two main sources of error in the data here: a standard error (SE) due to sample size (SE_N)

and resolution accuracy (SE_θ) of the OIM software. The sample size refers to the number

of disorientations obtained in a given OIM run. The SE_N was calculated using Equation

3.1 where x_i is the fraction of the sample size, N, contained in the ith bin of the rotation

angle histogram. The SE_θ was calculated using Equation 3.2. The total standard error

(SE_{TOT}) was then determined using Equation 3.3.

$$SE_N = \sqrt{\frac{x_i(1-x_i)}{N}}$$
Equation 3.1

$$SE_\theta = \frac{\theta_{RESOLUTION}}{\theta_{MAX}}$$
Equation 3.2

$$SE_{TOT} = \sqrt{(SE_N)^2 + (SE_\theta)^2}$$
Equation 3.3

The total standard error is plotted as a function of sample size in Figure 3.7(a) for

a histogram bar height equal to 0.1, which is 10% of the boundaries in a given

disorientation range corresponding to that histogram bin. As shown in this figure, the

total error asymptotically approaches the limit of resolution for the analysis system as the

sample size increases. Also shown in Figure 3.7 are examples of histograms with error

bars for (b), a constant resolution limit with varying sample size; and (c), a constant

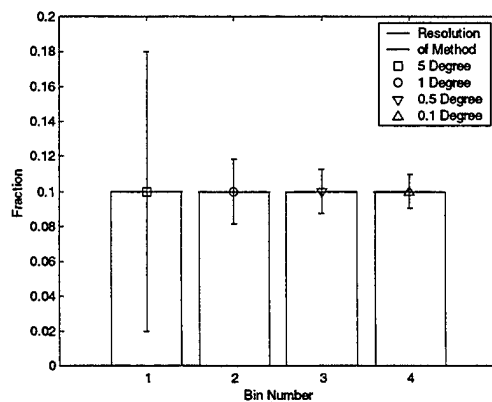sample size with varying resolution limit.

27

An advantage of OIM is the potentially large sample size, i.e. a large number of grain-to-grain disorientations, that may be obtained from a given sample. In contrast, TEM methods, which have potentially better resolution of grain-to-grain disorientations, generally include relatively small numbers of boundaries. Convergent beam electron diffraction (CBED) methods in TEM may provide resolution of 0.1° in disorientation measurements. The analysis conducted in this OIM research assumed a limit of resolution of 2° based on the accuracy stated in the technical documentation for this OIM system and a θ_{MAX} equal to 62.8°. With this resolution, the asymptotic limit of 0.0318 is essentially achieved after N = 1000 measurements are taken. The smallest sample size for rotation angle data included well over 2000 grain-to-grain disorientation measurements and this resulted in an error bar of +/- 0.032 being used for all histogram bar heights and subsequent polynomial fit curves for the rotation angle data. A representative example of a polynomial curve with error bars included is shown in Figure 3.8.
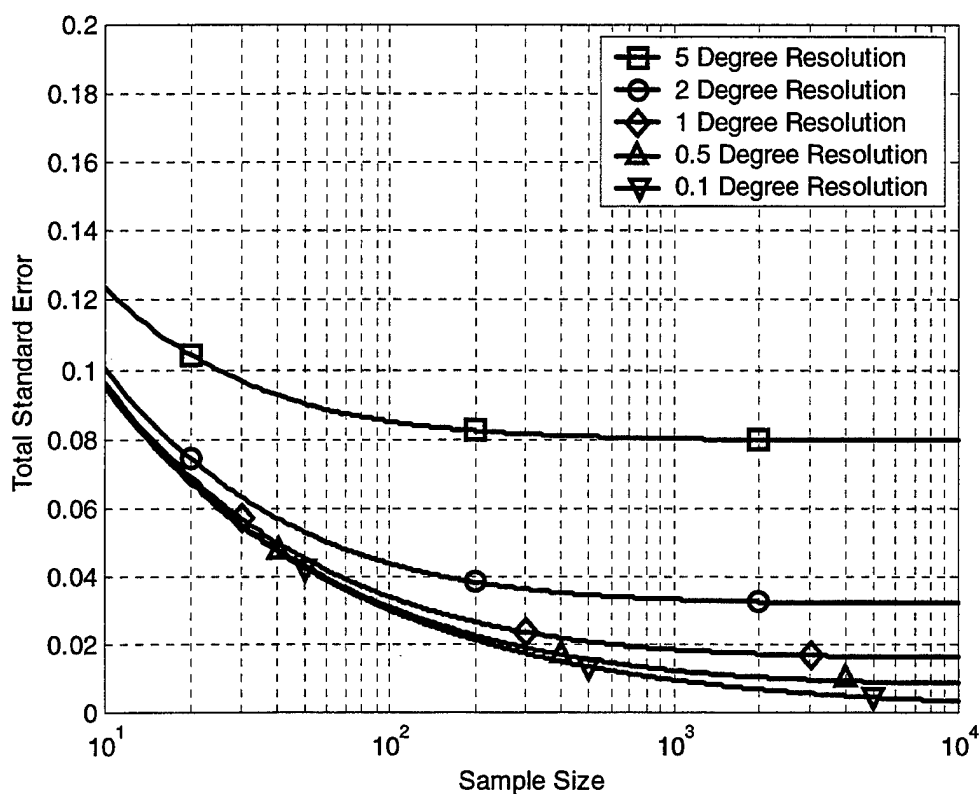
(a)
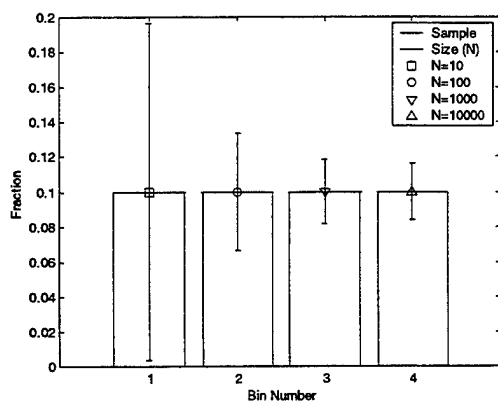
(b)

(c)

Figure 3.7. Examples of the error analysis for varying sample size and resolution limit. In (a), a plot of the Total Standard Error is shown for a histogram bar height (Fraction) of 0.10, for various resolutions of the disorientation as a function of the Sample Size; (b) shows Error Bars for various sample sizes using a uniform, 1° resolution; (c) example showing the Error Bars for various resolution limits with a constant sample size equal to 1000.
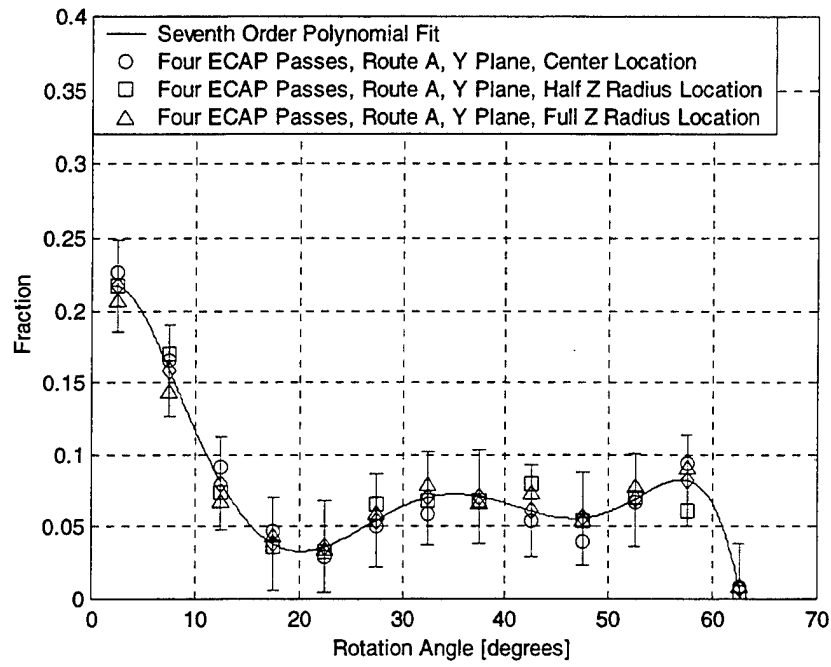
Figure 3.8. Representative example of polynomial fit data with associated error bars.

IV.   RESULTS AND DISCUSSION

A.   PURE ALUMINUM AFTER ONE ECAP PASS

The microstructure of this material after one ECAP pass is inhomogeneous. This may be seen from any of several viewpoints in the data. First, the OIM grain maps shown in Figures 4.1 and 4.2 indicate a large variation in the grain structure from region to region and there does not appear to be any particular dependence on position within the sample. Corresponding BSE micrographs, Figure 4.3, from the one pass material also indicate the inhomogeneity of the sample as well as the same general tendency of the grains to elongate in the shear direction that can be noted in the OIM results.   A comparison between the OIM grain maps and the BSE micrographs indicate regions that contain a single orientation, i.e., that consist of one grain, are often greater than 20 μm in extent. However, other areas can be identified in which a considerably smaller grain size may be discerned.

The rotation angle histograms shown in Figure 4.4 also exhibit significant differences among the regions examined and thus also suggest inhomogeneity of the microstructure as well. The variations among the histograms are consistently larger than the predicted standard error for any one run, based on the sample size and accuracy of orientation and disorientation determination.

The texture data, represented by the pole figures in Figure 4.5 and Figure 4.6, also indicate an inhomogeneous structure. Figure 4.5(a) shows texture data from a 20μm x 20μm region in which there is a single predominant orientation (e.g., there are only three prominent orientations in the 200 pole figure). Larger 100 μm x 100 μm regions (Figure

4.5(b) and Figure 4.6) may contain one dominant orientation, or multiple orientations. Additionally, the predominant orientation differs from one region to another. It can be seen in some cases that a [110] aligns with the shear direction (Figure 4.6(b)) and in others that [111] will align with the shear direction (Figure 4.6(a)); the shear direction is indicated by the dashed lines. It should also be noted that, in other areas, no low index pole is aligned with the shear direction.

In comparing the X plane data to the Y plane data, anisotropy of the microstructure is also apparent. The OIM grain maps and BSE micrographs indicate grain elongation in the direction of shear. The grain maps and micrographs from the X plane indicate elongation in the Y direction, which is parallel to the trace of the shear plane on the X face.

The histograms of grain-to-grain disorientation angles also indicate an anisotropic microstructure. Of particular note is the presence of peaks at 30° - 40° in the data obtained at the center and half-radius (along Y) positions on the X face. The data from the Y face suggest peaks in this same disorientation range but they tend to be smaller that those on the X plane.

Overall, these data indicate the presence of a large fraction of low-angle boundaries in the microstructure after one pressing pass. Thus, this is a deformation-induced structure for the most part, although some high angle boundaries are also evident. In addition to a peak in the distribution at disorientations of 30°- 40° the data suggest a second peak in some cases at 60°.

Figure 4.1. Grain Maps for pure aluminum processed by ECAP. The material has been subjected to one pressing pass. The relative locations on the Y plane of these 20μm x 20μm maps are indicated by the inset schematic. These grain maps illustrate the inhomogeneity of the microstructure in this condition.
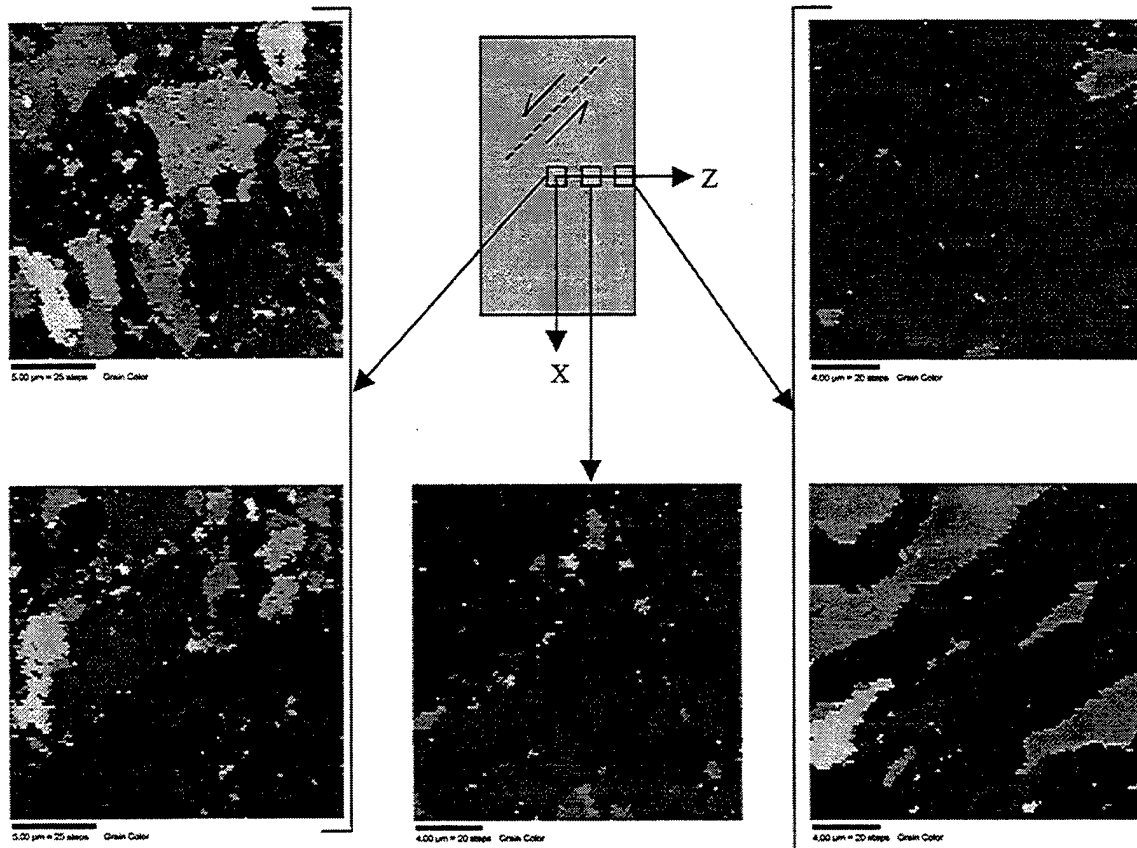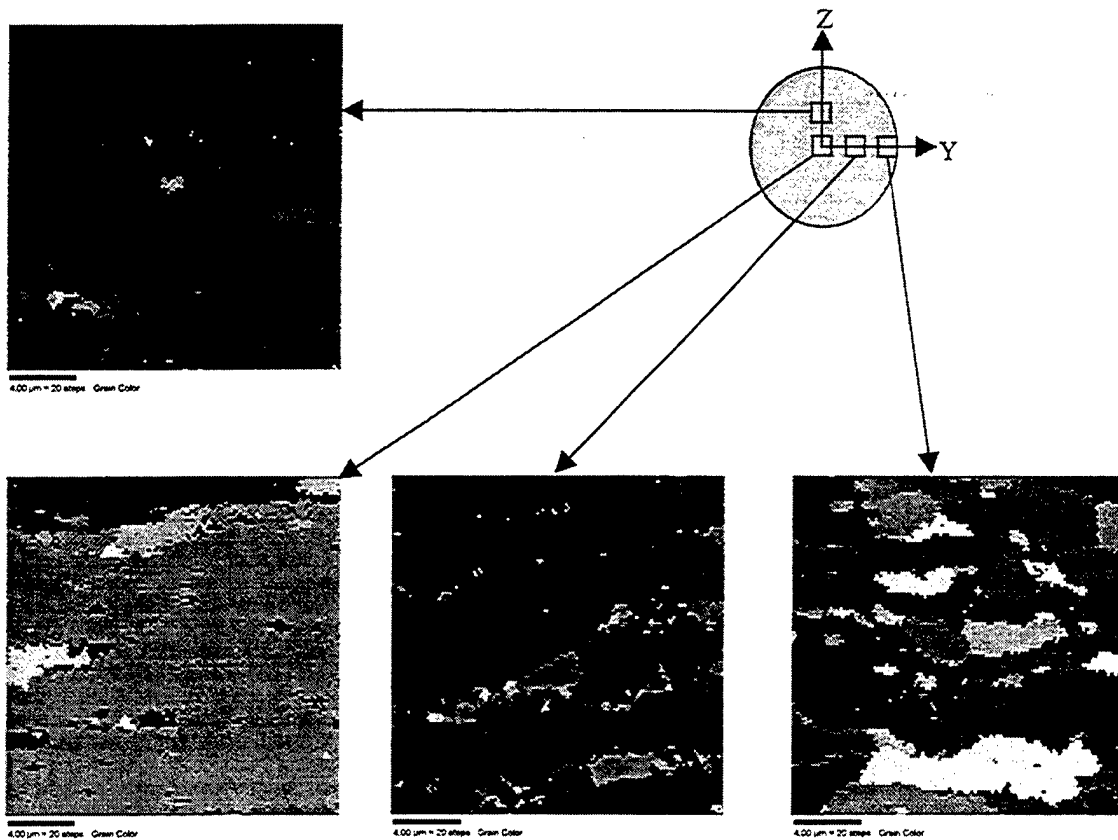
Figure 4.2. Grain Maps for pure aluminum processed by ECAP. The material has been subjected to one pressing pass. The relative locations on the X plane of these 20μm x 20μm maps are indicated by the inset schematic. These grain maps illustrate the inhomogeneity of the microstructure in this condition.
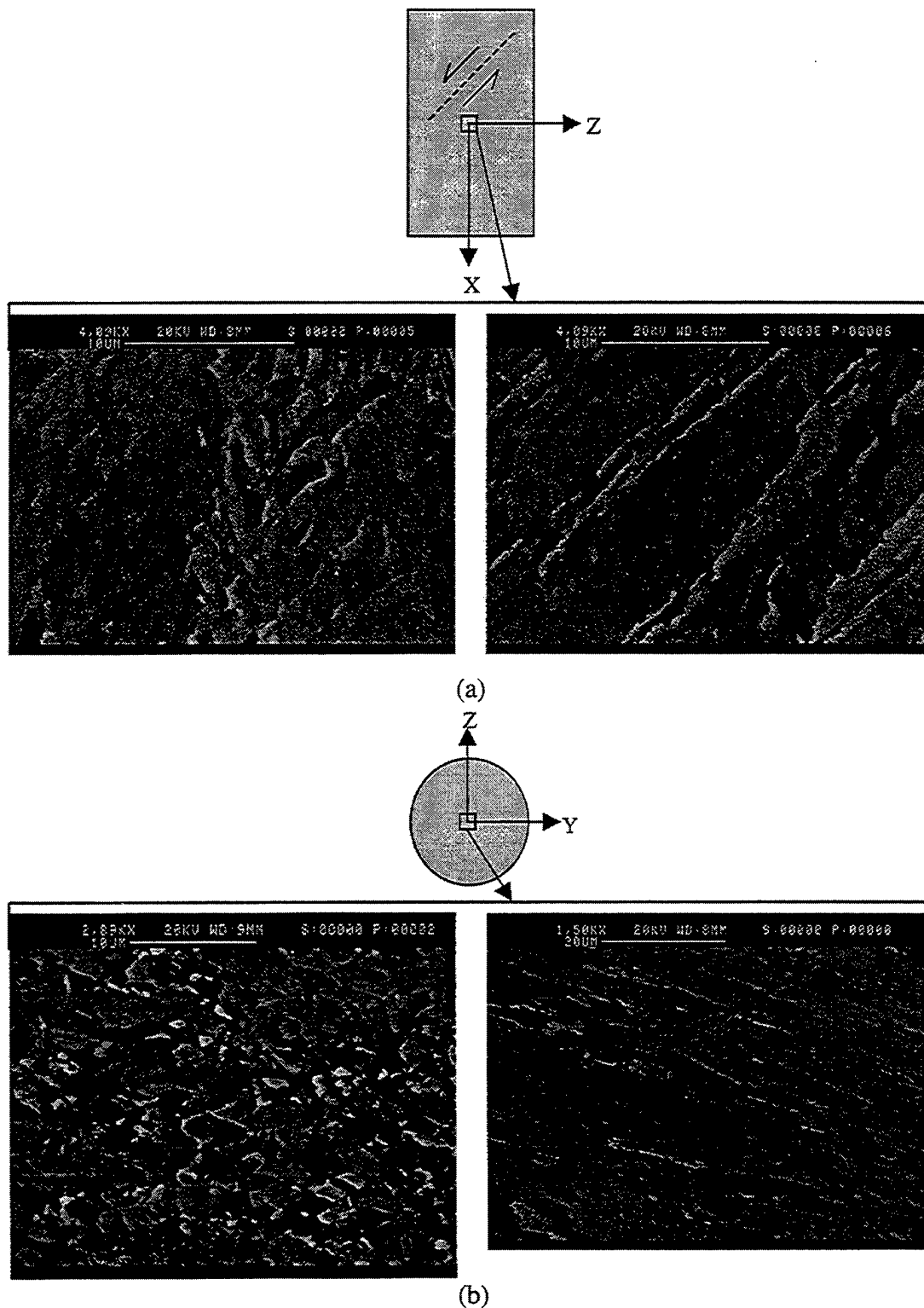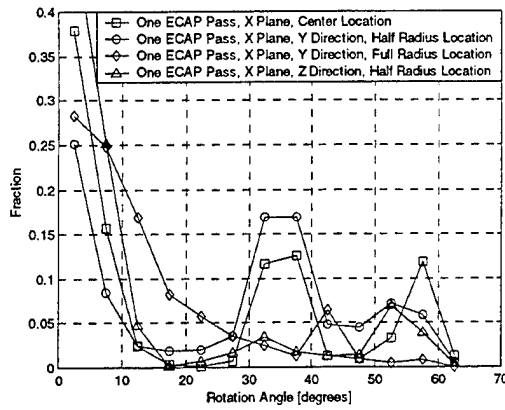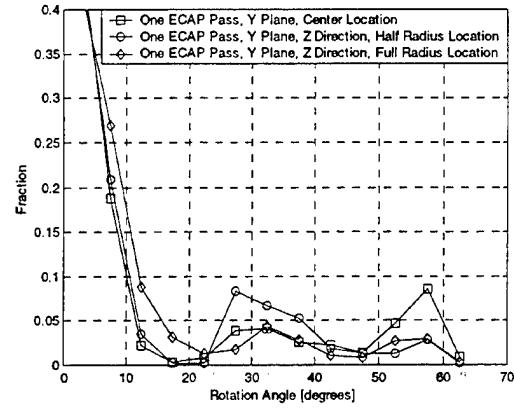
Figure 4.3. Back Scatter Emission (BSE) micrographs of aluminum after one ECAP pass. These micrographs illustrate the inhomogeneity of grain size after one ECAP pass in aluminum. Locations on the Y and X planes are indicated. These BSE images show orientation contrast with no etchant.

(a)   (b)

Figure 4.4. Relative fraction of boundaries as a function of rotation (disorientation) angle for pure aluminum after one ECAP pas. These data illustrate that most boundaries are low angle in nature and that the distribution is anisotropic. In (a), there is a distinct intermediate peak at 30°-40° for the X plane data at the center and half-radius locations. In (b), this intermediate peak is less distinct. In both cases, there is a peak at 55°-60°.

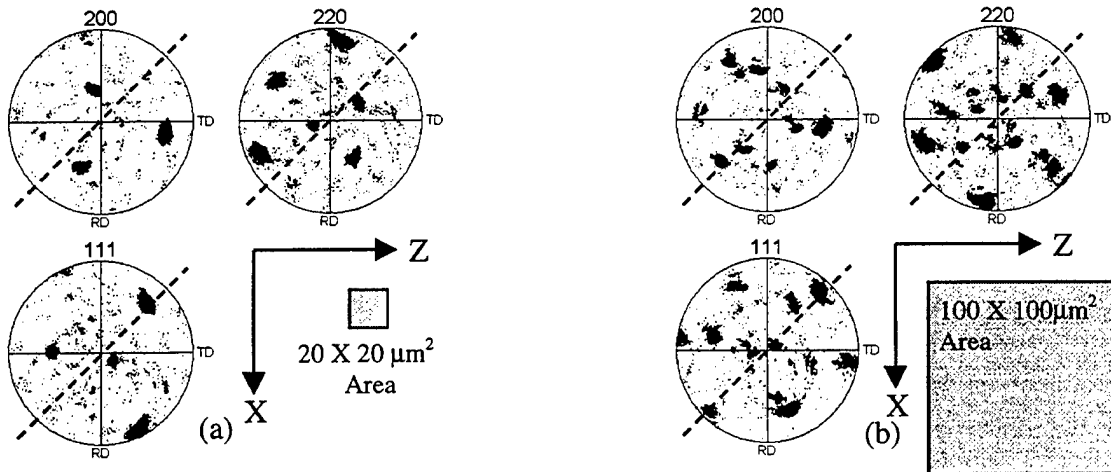
Figure 4.5. Representative pole figures from the center Y plane for ECAP aluminum after one pressing. In (a), a single dominant orientation within a small region is shown and (b) multiple orientations within a larger region. These figures illustrate the need for large and small area examinations in order to accurately represent the inhomogeneous nature of the microstructure in this sample.

36
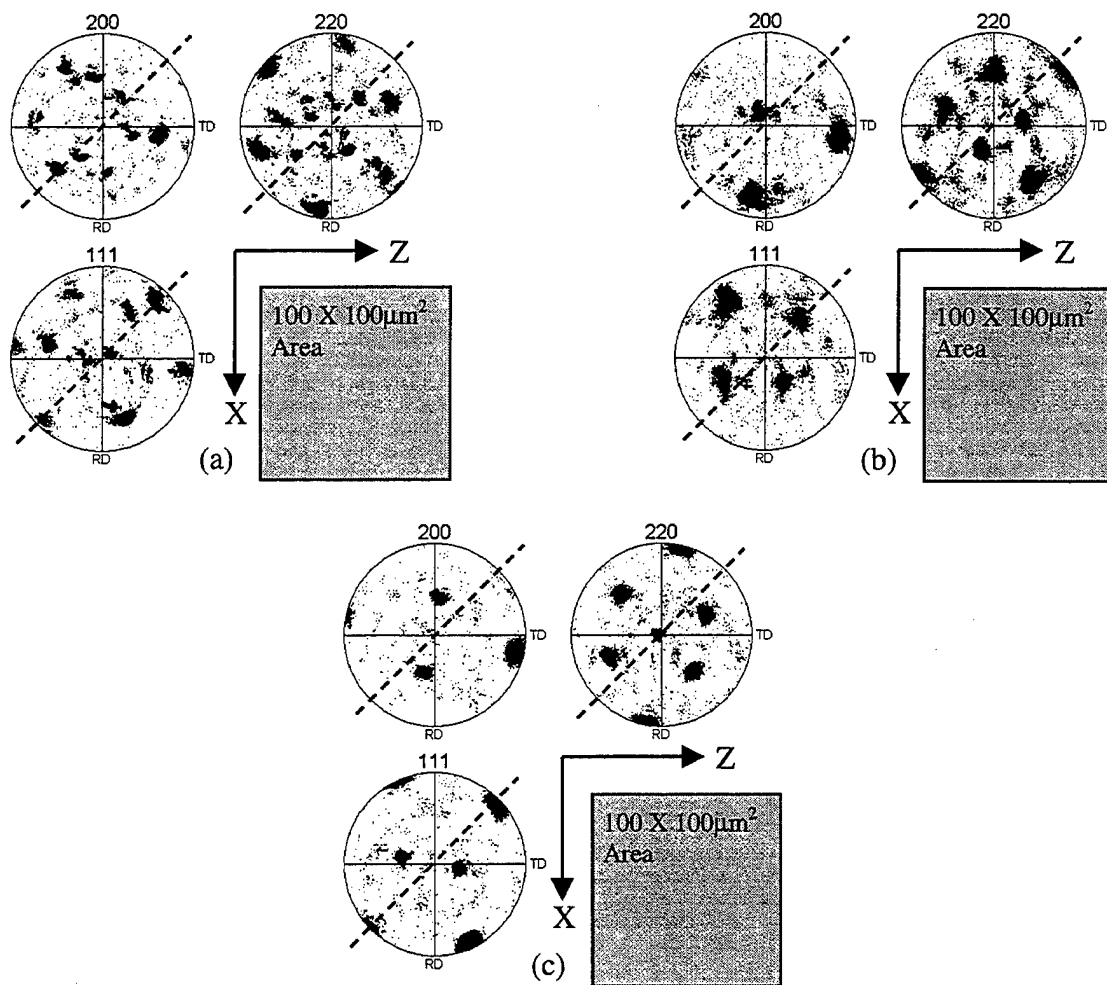
Figure 4.6. Pole figures from areas near the center of the Y plane in aluminum after one ECAP pressing operation. These figures illustrate the inhomogeneity after one pressing in that regions of similar size may contain either (a) multiple orientations, or a single dominant orientation as seen in (b) and (c). Additionally, in (a) and (c) a [111] is aligned with the shear direction {indicated by dashed lines}, and a [110] aligned with the shear direction is shown in (b).

B.   PURE ALUMINUM AFTER FOUR ECAP PASSES

After four ECAP passes the microstructure of this material is considerable more homogeneous than after the first pass alone. The OIM grain maps shown in Figure 4.7 are for material processed by route B_C, and indicate that both the grain size and the grain structure has been homogenized in both the X and Y planes, and to a similar degree in either plane. Alignment of the grains with the shear direction is evident in Figure 4.7(a), i.e., there is a persistent tendency of the grains to elongate in the shear direction of the last pressing operation. This grain elongation in the shear direction is evident at all locations examined from the center of the sample outward to the free surface along the Z axis. The apparent grain size and shape, however, are essentially independent of location on the Y plane. The grains on the X plane are also elongated in a direction parallel to the trace of the shear plane, i.e., in the Y direction, and this is evident in Figure 4.7(b). Comparison among the three microstructures in Figure 4.7(b) suggests some differences associated with location along the Y axis on the X plane. However, comparison of the data of Figure 4.7(b) with the microstructural data in Figure 4.2 suggests that these differences are much less after four passes than after the initial pressing pass. Finally, comparison of the microstructures in Figure 4.7(a) to those in Figure 4.7(b) indicate that the microstructure of this material is still anisotropic in nature after four pressing passes by route B_C.

The BSE micrographs shown in Figure 4.8 provide additional evidence of the trends shown in the OIM. Grain elongation along the shear direction is evident and the grain size apparent in the micrographs of Figure 4.8 is comparable to that evident in the OIM grain maps in Figure 4.7(a).

The influence of processing route is summarized in the OIM analysis presented in Figures 4.9 and 4.10. Material processed through four passes by route A exhibits a homogeneous microstructure in that the grain size and shape do not depend significantly upon position in the Y plane as shown in Figure 4.9. However, the grains become more nearly aligned with the X axis than with the shear direction for positions located at the half-radius and full-radius along the Z direction on this plane. Repetitive pressing by route A, for which there is no rotation of the billet between successive pressing passes, would result only in progressive rotation of the shear plane of the first pass about the Y axis. This rotation would continue until the shear plane for the first pass became parallel to the X axis. This is evident in Figure 4.9 for the microstructures obtained at the half-radius and full-radius positions along the Z axis. Friction with the die may account for the observation that the rotation of the shear plane toward alignment with the axis of the pressed sample becomes apparent near the surface for in route A material.

Grain maps from the center location of the Y face for samples pressed four times by each route of interest in this work are shown in Figure 4.10. There is little apparent difference in grain size and shape for these three processing conditions and all of these microstructures exhibit an apparent grain size of about 1.2 μm. This value is consistent with previous work [Ref. 17]. Furthermore, OIM grain maps and BSE micrographs that were produced for all routes demonstrated that the homogenization of the material did not appear to be dependent on processing route. For this reason further discussion of material processed by four pressing passes will be concerned only with route B_C.

Grain-to-grain disorientation angle data was for material pressed four times via route B_C is shown in Figure 4.11. These data were acquired from various locations on

either the X or the Y planes; within the uncertainty of measurement the data from either plane is identical and this supports the conclusion that the microstructure is essentially homogeneous after four pressing passes. However, the data obtained from the X face shows a distinctly larger population of boundaries disoriented by 30° - 40° when compared to the data from the Y face. In both cases the population of low-angle boundaries (e.g. 0° - 5°) has been reduced when comparison is made to the data for material subjected to a single pass (Figure 4.4). Indeed, this comparison suggests that the overall effect of repetitive ECAP is to shift the distribution of boundary disorientation angles upward in angle while retaining a preference for boundaries of 30° - 40° disorientation as well as 55° – 60° disorientation.

Microtexture data are shown in Figure 4.12 for each of these processing conditions. Data are presented for regions of two different sizes, 20 μm x 20 μm, i.e. the size of the regions scanned to produce the OIM grain maps, and from larger, 100 μm x 100 μm regions. The regions of larger size were scanned to assess meso-scale features in the microstructure. Overall the textures of these repetitively pressed materials have become more diffuse than those of material after one ECAP pass. This suggests an increase random component in the microstructure. In the data obtained from large, 100 μm x 100 μm regions for materials processed by either route A or B_C, there is a strong tendency for a <111> to align with the direction of shear in the last pressing operation. In contrast, there appears to be rotational symmetry about a <111> that lies near the Y direction in the shear plane; this is most evident in Figure 4.12(f).

All scans from the larger, 100 μm x 100 μm regions show clear evidence of multiple orientations. The relative intensities associated with each of the orientations are

approximately equal for material processed by routes B_C and C, as seen in the Figures 4.12(d) and (f). On the other hand there is one dominant and multiple lesser orientations in Route A in the data of Figure 4.12(b). Lastly, the scans from the smaller, 20 μm x 20 μm regions tend to be somewhat less diffuse in nature and may only contain one dominant orientation that is similar to that present in material after one pressing pass. This suggests that there are meso-scale features in the microstructures of these repetitively pressed materials that warrant investigation on the larger scale. This is consistent with the data for this material after the initial pressing pass. In some cases multiple orientations were observed while in others only a single orientation was evident. Again, this indicates that there are likely meso-scale features that may have been missed in the scans on material subjected to one ECAP pass.
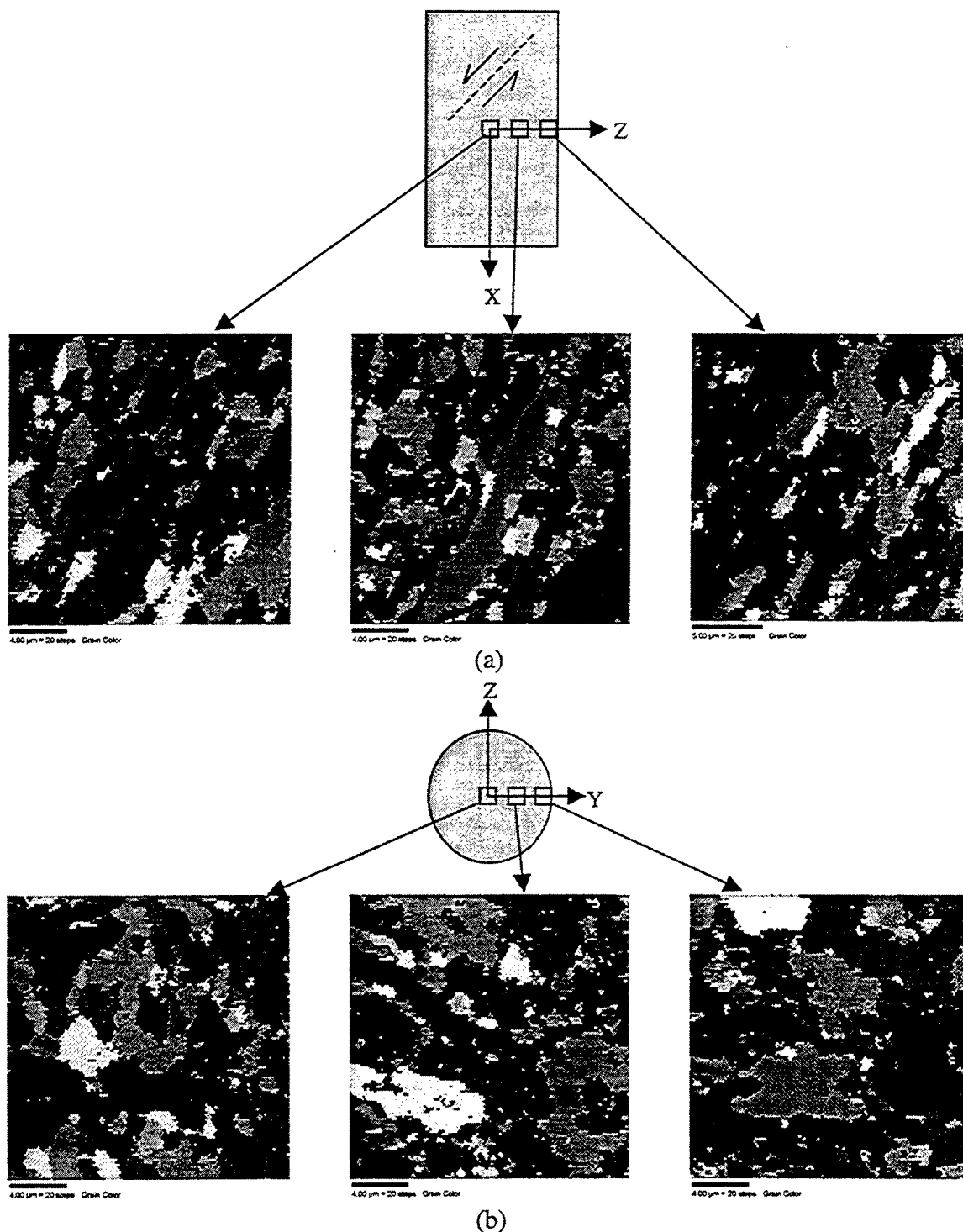
Figure 4.7. Grain maps produced by OIM analysis of ECAP aluminum pressed four times following Route B_C. The relative locations of these 20μm x 20μm maps on the Y and X planes are illustrated by the inset schematics from (a) the central Y Plane and (b) X Plane. Homogenization is also evident for repetitive pressings by Route B_C, however, comparison of the (a) Y plane and (b) X plane, the anisotropic nature of the microstructure is revealed.
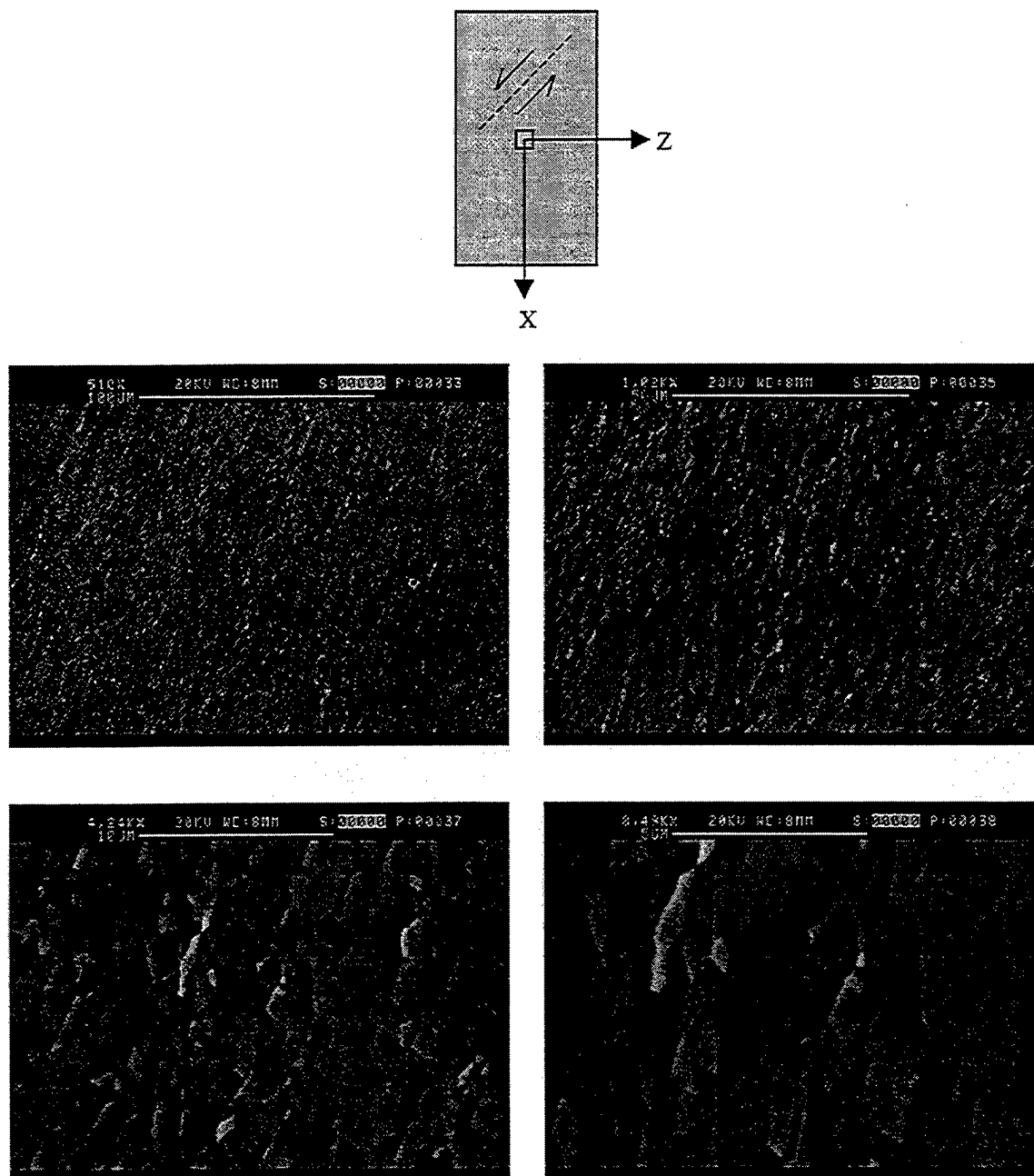
Figure 4.8. BSE Micrographs of pure aluminum after four ECAP passes via Route B$_C$. These micrographs are all from the same approximate location at the center of the Y plane. Comparison with Figure 4.7 (a) illustrates the homogenization of the microstructure with additional strain; also there is good agreement with the OIM grain maps regarding grain size, orientation and homogenization.

43

Figure 4.9. Grain Maps for pure aluminum processed by ECAP after four pressings by Route A. The relative locations of these 20μm X 20μm maps on the Y plane are indicated in the inset schematic. These maps illustrate increased homogeneity of the microstructure as reflected in both grain size and shape throughout the sample.

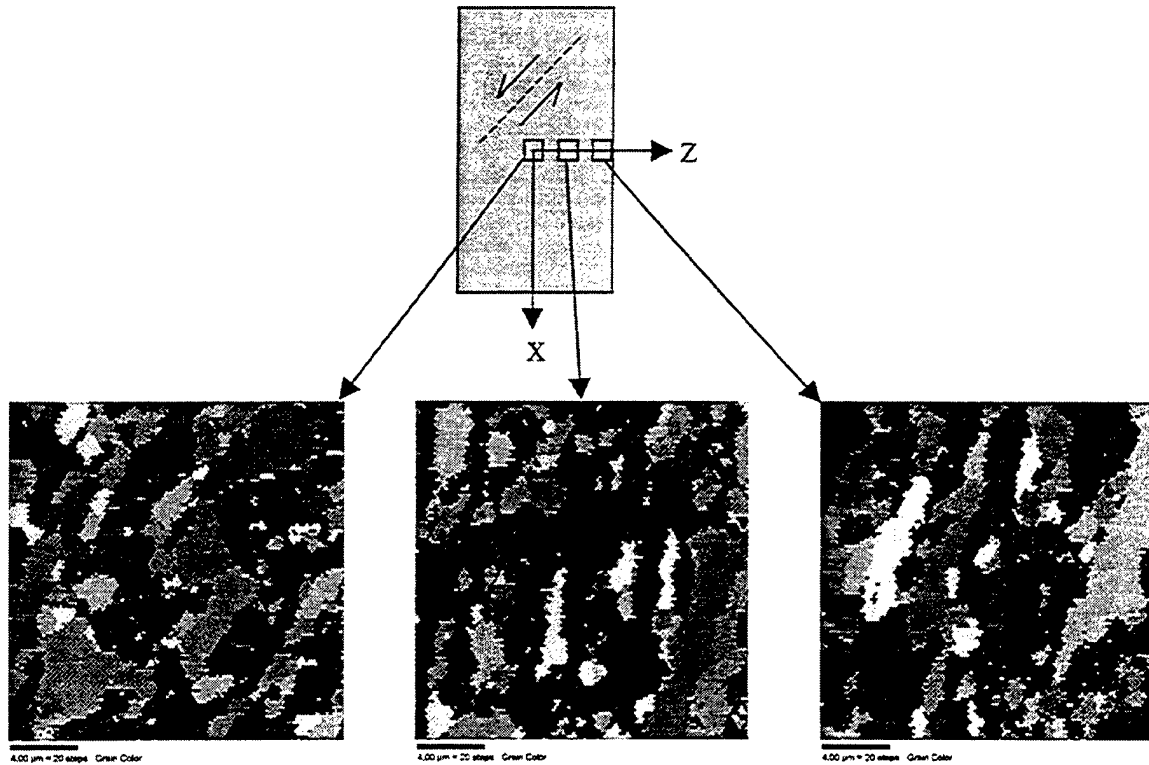(a)   (b)   (c)
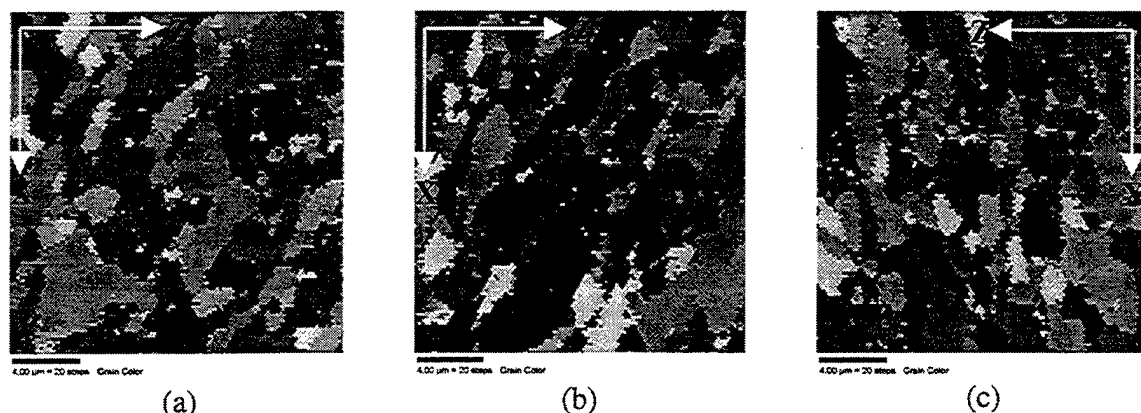
Figure 4.10. Representative Grain Maps for pure aluminum processed by ECAP after four passes. In (a), Route A; (b), Route B_C and (c), Route C are represented. Note that the grain size is more uniform than in material pressed only once and that grains are elongated in the direction of the last shearing process. There is very little difference in grain size between the various routes.

(a)   (b)
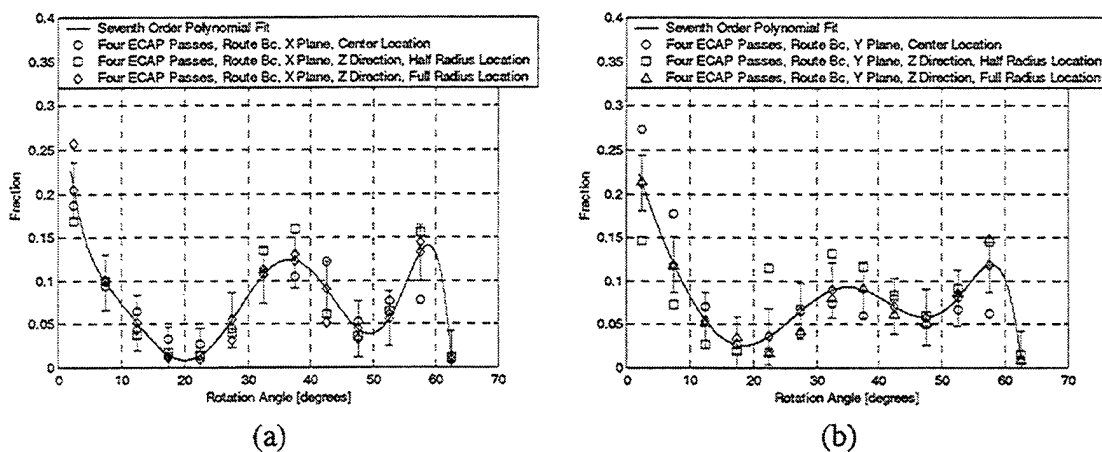
Figure 4.11. Rotation angle data that have been fitted to a Seventh Order Polynomial using a least squares approach for ECAP aluminum that has been pressed four times. In (a) the X plane data are represented and in (b), the Y plane data. The small variation in the data points leads to the conclusion that at four pressings and beyond, the material has completely homogenized with respect to rotation angle distribution.
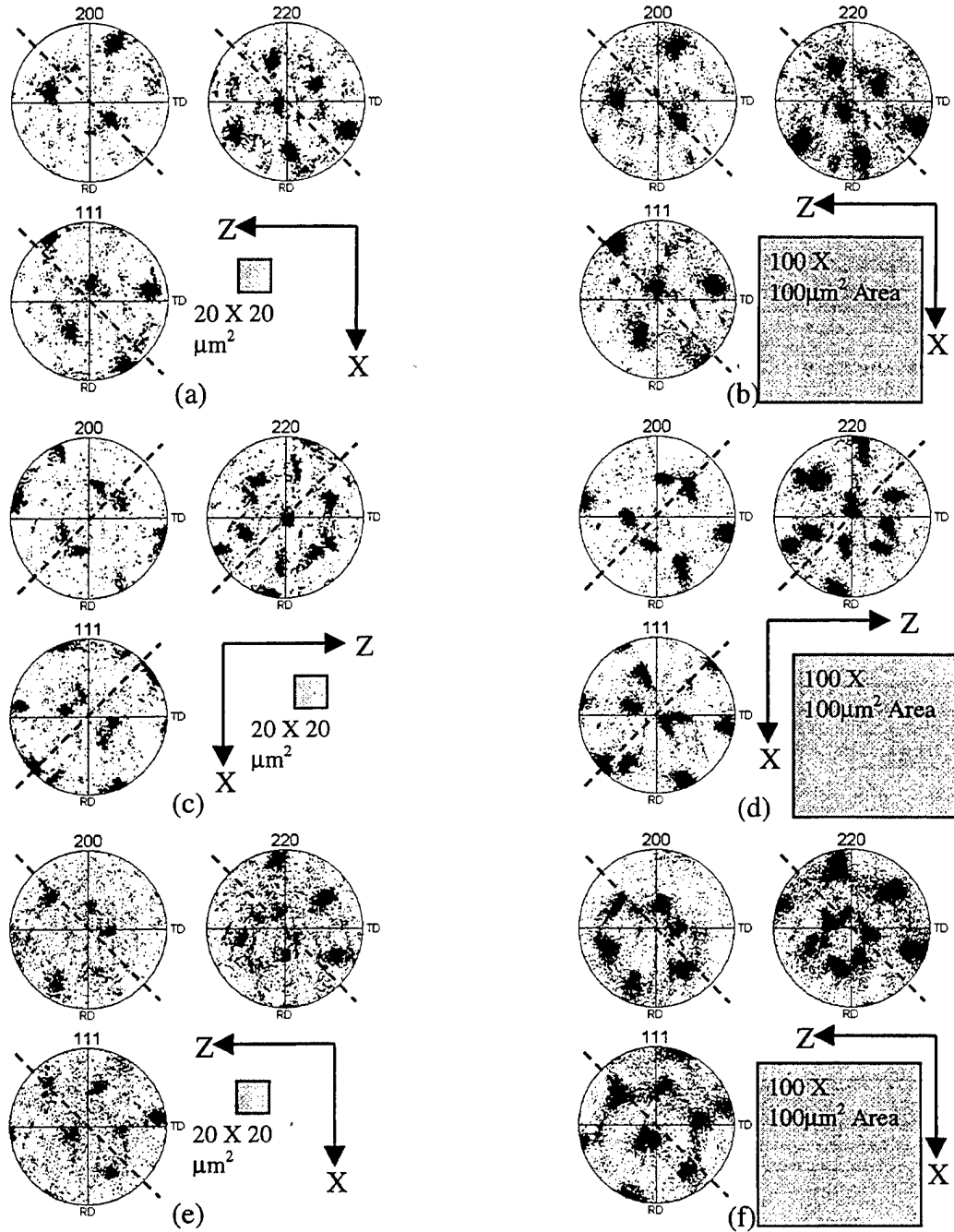
Figure 4.12. Representative pole figures near the center of the Y plane for ECAP aluminum after four pressing operations by: (a) and (b) Route A, (c) and (d) Route B$_C$, (e) and (f) Route C. All routes lead to a more diffuse orientation distribution irrespective of the size of the area scanned, indicating a dependence on the number of pressings. The small area scans (a) and (c) indicate only one dominant orientation, while (b) shows two orientations of almost equal strength. The large area scans (b), (d) and (f) all show two orientations, but to a lesser degree as noted in (b).

C. PURE ALUMINUM AFTER TWELVE ECAP PASSES

Repetitive ECAP is intended to provide a refined, homogeneous microstructure that includes high-angle grain boundaries. Microtexture and OIM data were acquired on pure aluminum that had been subject to twelve ECAP passes via routes A, B_C and C. These data were obtained, as before, on the X and Y planes of as-pressed samples in order to assess grain refinement and nature of the grain boundaries.

Grain maps for material processed by route B_C are presented in Figure 4.13. These maps from the Y plane show that the grains are elongated in the shearing direction for the final pressing pass although comparison with Figure 4.7(a) indicates that the grain aspect ratio tends is less than that for material processed by four ECAP passes via route B_C. Thus, the additional pressing passes have resulted in a more equiaxed grain structure but mean linear intercept measurements suggest that the grain size has remained essentially unchanged at about 1.2 μm after 12 ECAP passes. There is no apparent dependence on location in the sample and so repetitive pressing has provided a homogeneous microstructure. The same observations can be made in respect of the OIM grain maps obtained from the X plane shown in Figure 4.14. For these data the elongation of the grains is again in a direction that is parallel to the trace of the shear plane, which is the Y direction on the X plane. A high degree of microstructural homogenization is apparent and there is no evidence of recrystallization via the formation of new grains and long-range migration of high angle boundaries. Also, there do not appear to be any effects evident in the microstructures obtained near the billet surfaces that would reflect die friction effects.

Figure 4.15 illustrates the effect of processing route and compares OIM grain maps for materials processed by routes A, B_C and C. In all cases alignment of the grains with the shear direction of the final pressing pass is evident. However, the grain size is essentially independent of pressing route and the same degree of homogenization was apparent for all three pressing procedures.

Grain boundary data in the form of rotation angle histograms are provided in Figure 4.16 that is for material processed by twelve ECAP passes using route B_C. Comparison of the data of Figure 4.16 with those of Figures 4.4 and 4.11 shows that the population of low-angle boundaries generally decreases as the number of pressing passes increases. Nevertheless 20% - 30% of the boundaries are still low-angle in nature ($2° < \theta < 15°$) after 12 pressing passes, which reflects a prominent population of deformation-induced boundaries. In common with previous rotation angle data for material processed by either one or four ECAP passes, it is evident that there is a persistent anisotropy when data for the X and Y planes are compared. In essentially all of the X plane data (Figures 4.4(a); 4.11(a); and 4.16(a)) there is a prominent peak at ~35° that develops in the initial pressing and then persists through 12 passes. As noted earlier, this peak is not evident in some of the scans for material that has experienced only one pressing pass due to the inhomogeneous nature of that condition. In contrast, a similar peak for data on the Y plane is observed at ~30° for the material after one pass (Figure 4.4(b)). The disorientation angle for this peak increases to ~35° after four pressings (Figure 4.11(b)) and increases again ~38° after twelve pressing passes (Figure 4.16(b)). Furthermore, the height of this peak is consistently lower for the Y plane data. Finally,

48

both the X plane and Y plane data indicate a high-angle peak at 55° - 60°, which is prominent in all of the data for materials experiencing four or more pressing passes.

Microtexture data for material processed through 12 ECAP passes are shown in Figure 4.17. Data for all three processing routes are included. Comparison with Figure 4.12 indicates that increasing the number of pressing passes from four to 12 results in still more diffuse orientations distributions; this especially evident in the larger area scans. The smaller area scans may show a dominant single orientation while the larger area scans generally show multiple orientations, indicating that there are meso-scale features in these microstructures. Careful examination of the larger area scans reveals axes of rotational symmetry in all of these data. For material processes by route A, there appears to be rotational symmetry about the shear plane normal; this is most evident in the {220} pole figure in Figure 4.17(b). In this figure there is a prominent band of orientations perpendicular to the shear plane and a corresponding band parallel to the shear plane in the {111} pole figure. Other orientations are also evident in these data; these additional orientations may be carried over from prior pressing passes. The pole figure data for material processed through 12 ECAP passes via route B_C (Figure 4.17(d)) also exhibits rotational symmetry about an axis normal to the shear plane of the final pressing pass. However, in this case a <110> is aligned with this rotation axis, giving rise to a high concentration of orientations at a position normal to the shear plane in the {220} pole figure. There is a second band in the {220} pole figure for this condition that suggests rotation about an axis inclined at 45° to the shear plane in the Z direction. The rotation axis may be <111>, as reflected in the orientations at this location in the {111} pole figure for this condition. Rotational symmetry about a <110> is also evident in material

49

processed by route C, but now the rotation axis is nearly aligned with the X axis, i.e., with the axis of the as-pressed billet. The resulting fiber texture is incomplete in that the bands associated with the rotation axis do not exhibit a continuous distribution of orientations.

Figure 4.13. Grain maps for pure aluminum processed by ECAP. The material has been subjected to twelve pressing operations via Route B_C. The relative locations on the Y plane of these 20μm x20μm maps are indicated by the inset schematic. These grain maps confirm the continued homogenization of the structure with slight grain elongation in the direction of shear from the last pressing operation.
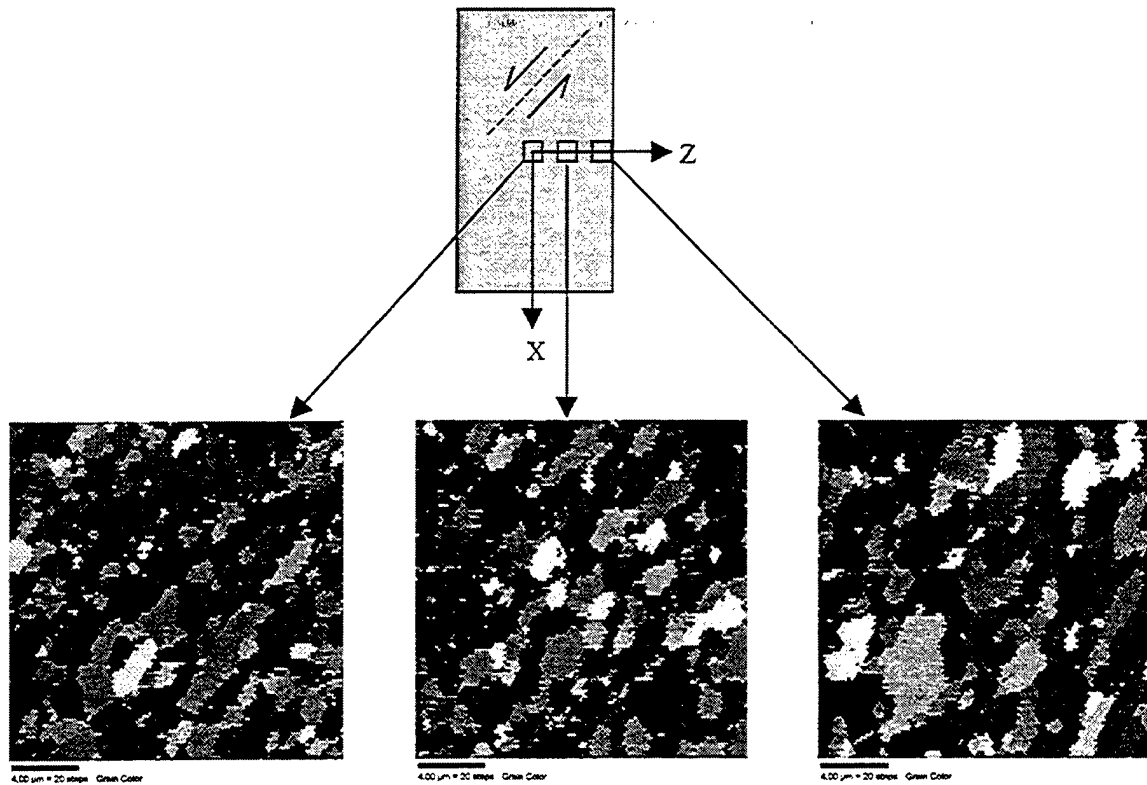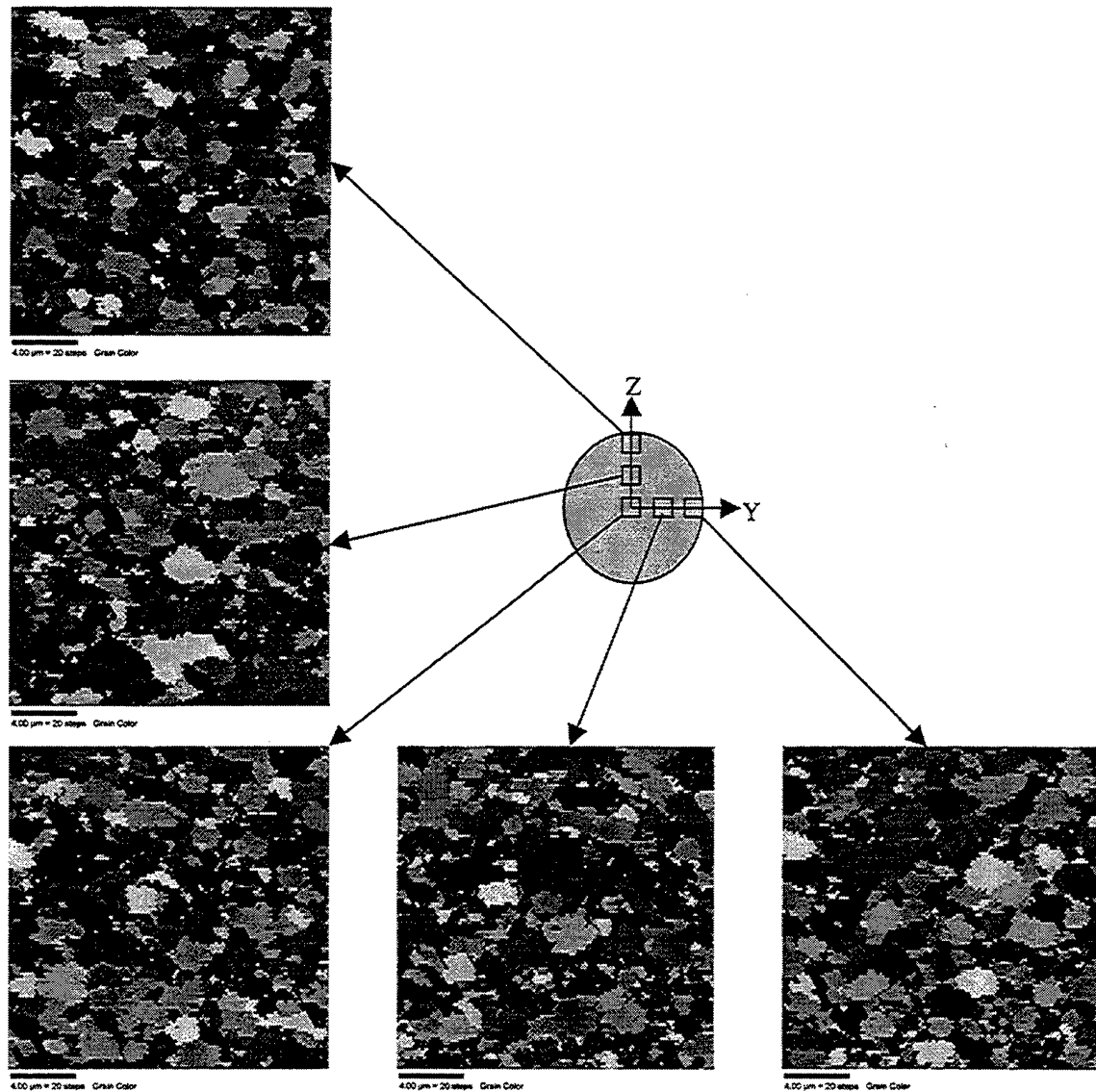
Figure 4.14. Grain maps for pure aluminum processed by ECAP. The material has been subjected to twelve pressing operations via Route B_C. The relative locations on the X plane of these 20μm x20μm maps are indicated by the inset schematic. The grains tend to be elongated in the Y direction, which is parallel to the trace of the shear plane on the X face of the material.

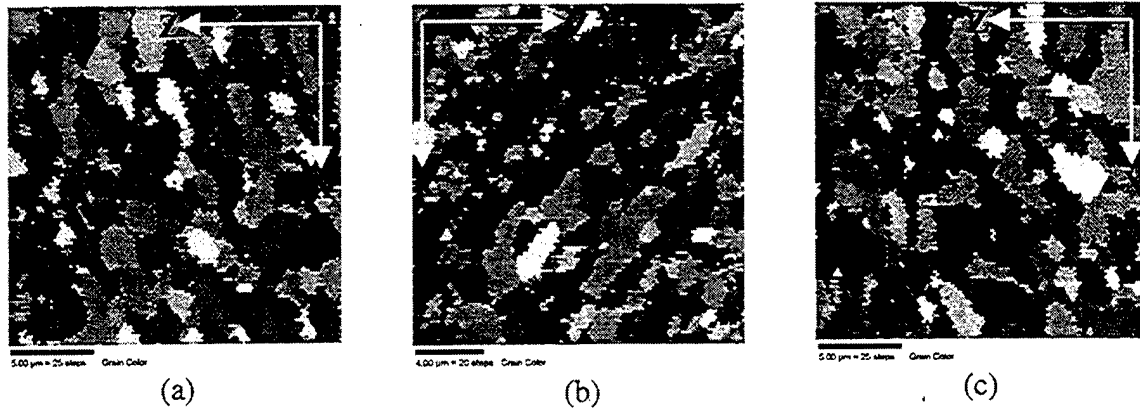(a)   (b)   (c)

Figure 4.15. Grain maps for pure aluminum processed by ECAP. The material has been subjected to twelve pressing operations via various routes. In (a), Route A; (b) Route B_C and (c) Route C is represented. As seen in Figure 4.10, there persists a tendency for grain elongation in the direction of the final shearing in the ECAP process; there is little difference in the grain size for the various routes. The grain size of (b) Route B_C is in keeping with previously reported sizes and elongation characteristics.

(a)   (b)
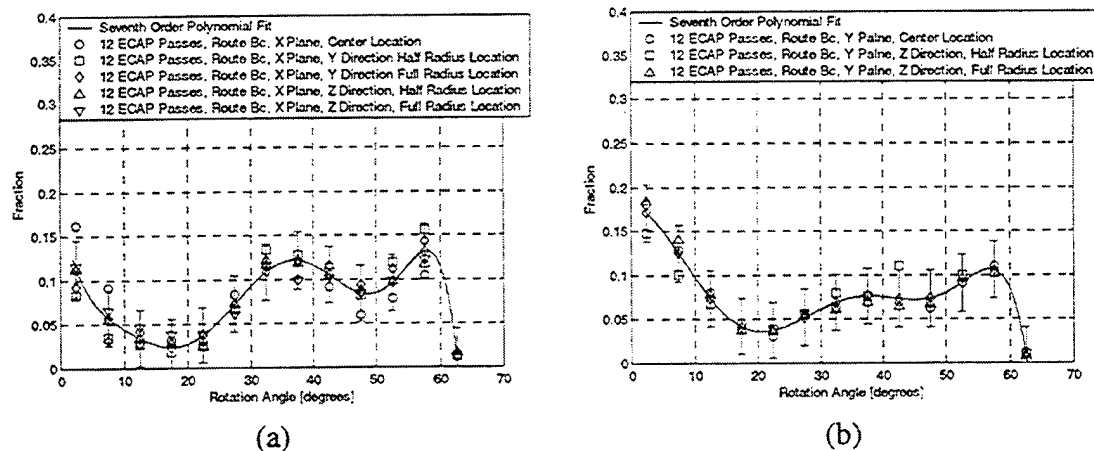
Figure 4.16. Representative rotation angle data of Twelve ECAP Passes on the (a) X and (b) Y Planes. The trends in the histograms indicate a consistent peak at approximately 35° on the X Plane data in comparison to Figures 4.4 (a) and 4.11(a). When compared to Figures 4.4 (b) and 4.11 (b), the (b) Y Plane data shows a peak of equal or lesser magnitude that tends to increase in rotation angle from ~32° in Figure 4.4 (b) to ~35° in Figure 4.11 (b) and finally to ~39° presented here. This 30-40° peak is the anisotropic evidence.

52
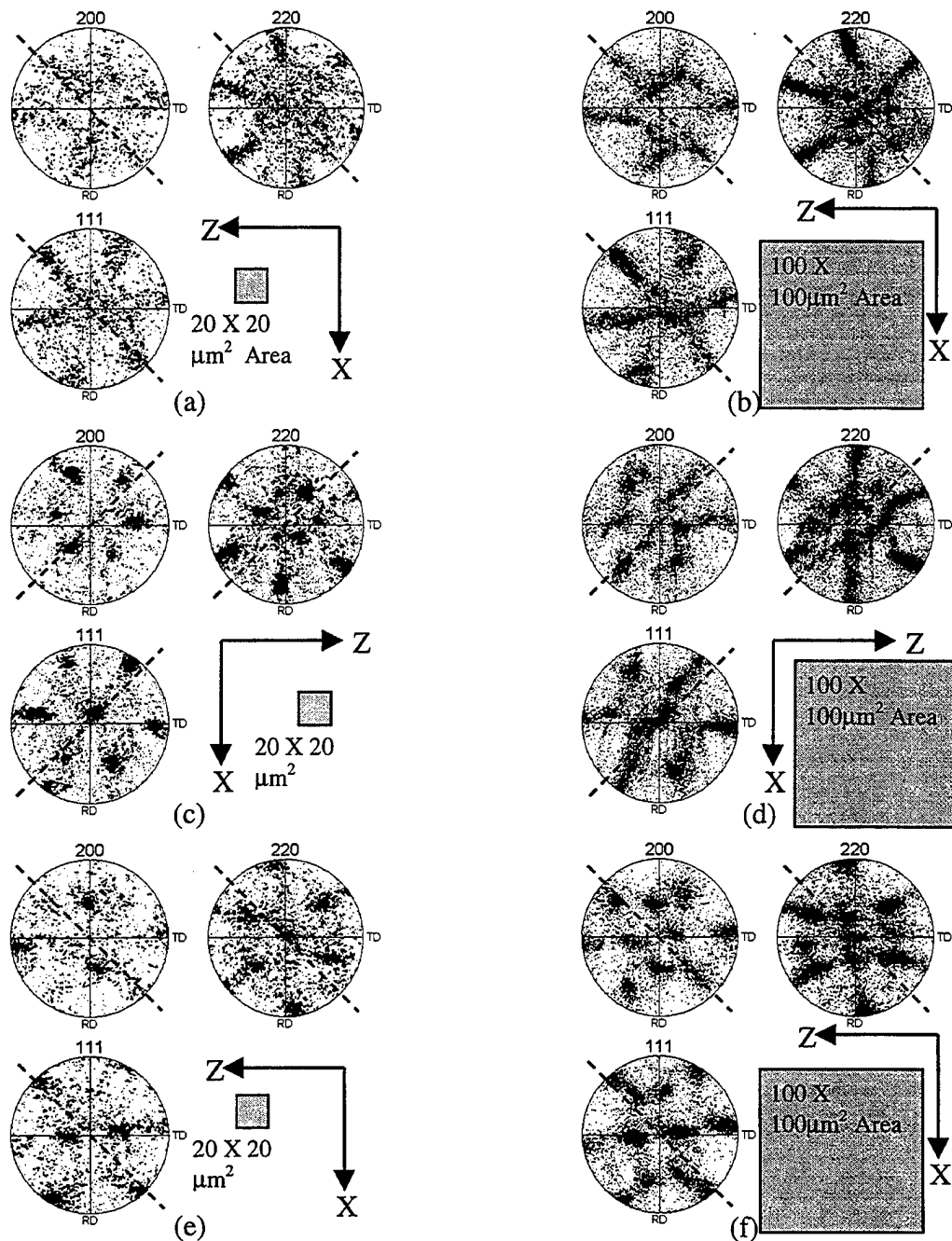
Figure 4.17. Representative pole figures from the center of the Y plane in ECAP aluminum after 12 pressings. Data in (a) and (b) Route A, (c) and (d) Route B_C, (e) and (f) Route C. The orientations tend to become even more diffuse with repeated pressings. As shown in previous Figures 4.5, 4.6 and 4.12, the small area scans (a), (c) and (e) have a greater tendency to only contain a few dominant orientations, while the larger areas (b), (d) and (f) yield results of the meso-scale texture of the material. Of note to all pressing operations, a [111] tends to align with the shear direction as indicated by the dashed lines.

D.   UNIQUE FEATURES, DEFORMATION BANDING

The pole figure data presented in Figures 4.5, 4.6, 4.12 and 4.17 often indicate the presence of at least two distinct orientations. This is especially the case for scans that acquire data from the larger 100 µm X 100 µm regions. Unlike X-ray diffraction methods, which acquire data from a large volume of material simultaneously, microtexture analysis in OIM includes texture determination by a succession of grain-specific orientation measurements. Because the position of the orientation measurements is recorded along with the orientation data themselves it is possible in OIM to code the data to reveal the distribution of the orientations within the grain maps. This may be accomplished by color coding of orientations within some tolerance of a selected orientation. Figure 4.18 provides an example of this analysis of material processed through four ECAP passes via route B_C. The corresponding pole figure data is the same as that of Figure 4.12(d), but now each of the two distinct orientations in these data have been separately highlighted.

Careful examination of the {200} pole figure in Figure 4.18(a) suggests that the two orientations (one is gray, the other black) are approximately related by a mirror operation where the mirror plane is the shear plane. Alternatively, these orientations may be related by a rotation of approximately 60° about a <110> that is aligned with the Y axis in the shear plane. Coding the grain map to correspond to these two orientations (within a ± 10° tolerance) reveals a distinct band structure as shown in Figure 4.18(c). The bands are regions in the material in which the lattice orientation corresponds to one or the other of the two distinct orientations noted in the pole figure data. Furthermore, these bands are aligned with the shear plane and the lattice orientation within each band

alternates between the two symmetric orientations along a direction normal to the shear plane. Especially noteworthy is that the high-angle boundaries in the disorientation distribution (Figure 4.18(b)) correspond to the interfaces between these bands. The region of interest in Figure 4.18 was scanned using a 1.0 μm step size and so the resolution is insufficient to reveal the finer-scale grain structure and associated boundaries. For this reason, only disorientations ≥ 20° were included in this analysis.

The arrangement of the band-like features in Figure 4.18(c) is suggestive of the deformation-banding model of microstructural development during severe rolling deformation [Refs. 28-34]. Deformation banding represents a mechanism of grain subdivision during severe deformation in which the lattice on opposite sides of the band interface rotates in opposite senses. The material in each band may be able to deform with fewer than five independent slip systems and this reduces the extent of dislocation intersection processes and results in less work expenditure during deformation. However, sufficient work must done to create the band/band interfaces. In analysis of banding during rolling, Hirsch and Lücke [Ref. 35] have concluded that an alternating sequence of bands is necessary because each band may not deform in plane strain as dictated by the rolling reduction. Simply arranging the bands in an alternating sequence may allow accommodation of the additional shear strains, which themselves alternate in sense, that arise separately in each band.

An alternative representation of the alternating character of the lattice orientation is illustrated in the plots of Figure 4.18(d) and (e). In both cases the plots correspond to the linear traverse along the Z axis as indicated in the map of Figure 4.18(c). In 4.18(d) the disorientation of each point along the traverse is determined relative to the origin of

55

the traverse. Here it is clear that the orientation alternates back and forth between two separate orientations in the texture. It must be kept in mind that disorientations are always taken as absolute values and so the true disorientation corresponding to steps from one band to the next may not be reflected in this representation. Alternatively, the point-to-point disorientations may be plotted as shown in Figure 4.18(e). These data suggest two different sets of disorientation values: 55° - 60°, and 30° - 40°; these ranges correspond to the two peaks noted earlier in the discussion of the disorientation data for this condition (Figure 4.11). Of particular note is that the width of the alternating bands is 20 µm – 25 µm while the bands appear to extend hundreds of microns in the material, indicating the presence of meso-scale features that would be difficult to detect by more highly resolving techniques such as TEM.

Scans at higher resolution over areas roughly corresponding to the width of these bands are shown in Figures 4.19 and 4.20. These were both acquired from the same region as Figure 4.18 and utilized step sizes of 0.2 µm. The grain maps were again coded by the aforementioned highlighting technique in order to aid in microstructural analysis.

Figure 4.19 shows a region near a band/band interface which is located just to the left of center in the map. Again, the band/band interfaces correspond to the high-angle boundaries in the disorientation distribution shown in Figure 4.19(b). Now, with the higher resolution in these data the low-angle boundaries in the disorientation distribution can also be identified and correlated with location in the orientation map. The low-angle boundaries are seen to be located in the interior of the bands and this indicates the presence of a sub-structure within the bands. Thus, the bands consist of cells or subgrains

56

separated by low-angle boundaries and the presence of this cell or subgrain structure accounts for the spread of orientations evident in the pole figure data. Figure 4.20 provides a separate example of this same low angle sub-structure that resides within the bands. However, the pole figure and orientation map for this example indicates only one dominant orientation in the region examined. Thus a complete picture of the microstructure of this material cannot be obtained from regions smaller that the dimension of these bands.

Deformation banding has also been proposed to describe the development of microstructure in an Al-Cu-Zr alloy, Supral2004 [Ref. 36]. The same data acquisition, clean up and analysis techniques were used in the examination of microstructure in rolled Supral 2004 which had been subjected to an annealing treatment. A simplified schematic of the rolling process and definition of the plane examined by OIM is shown in Figure 4.21.

The data for Supral 2004 are shown in Figure 4.22. Again, two dominant orientations are apparent in the texture. The texture is a rolling texture with a predominant B (or Brass) type component; this component consists of orientations near {110}<211> where this notation refers to {rolling plane}<rolling direction>. There are two symmetric variants of this texture and these are the dominant orientations highlighted in Figure 4.22(a). The grain map documents the presence of bands in the microstructure in which the lattice alternates back and forth between orientations corresponding to the symmetric variants of the B texture component. This analysis was again conducted with a tolerance of ± 10° in orientation. As also noted in the ECAP data, the high-angle boundaries in the disorientation distribution correspond to interfaces between the bands.

57

In fact, it is straightforward to show that the symmetric variants of the exact B texture component are related by a 60° rotation about a <111> that is aligned with the TD. It should be noted here that there is a significant difference in the width of the bands in comparison to those observed in the ECAP material. In this 20μm x 20μm examined area, the width of the bands is about 2 μm – 4 μm. Additionally, the bands tend to be less continuous over a long distance in the RD. However, the low-angle boundaries are again associated with a cell or subgrain structure within the bands and this is consistent with the results for the pure aluminum after ECAP processing. Figure 4.23 shows point-to-origin and point-to-point disorientations for a linear traverse oriented along ND in the microstructure. Again, the bands are shown to alternate between two equivalent orientations and the band interfaces are the high-angle boundaries of 50° - 60° disorientation.

The above observations lead to the conclusion that deformation banding has now been observed in a pure metal and in an aluminum alloy, and associated with two different processing methods. This suggests that it is a general phenomenon related to large strain plastic deformation. The size (thickness) and contiguity of the bands may be significantly affected by processing technique, type and quantity of alloying elements and the size of any second phase particles.
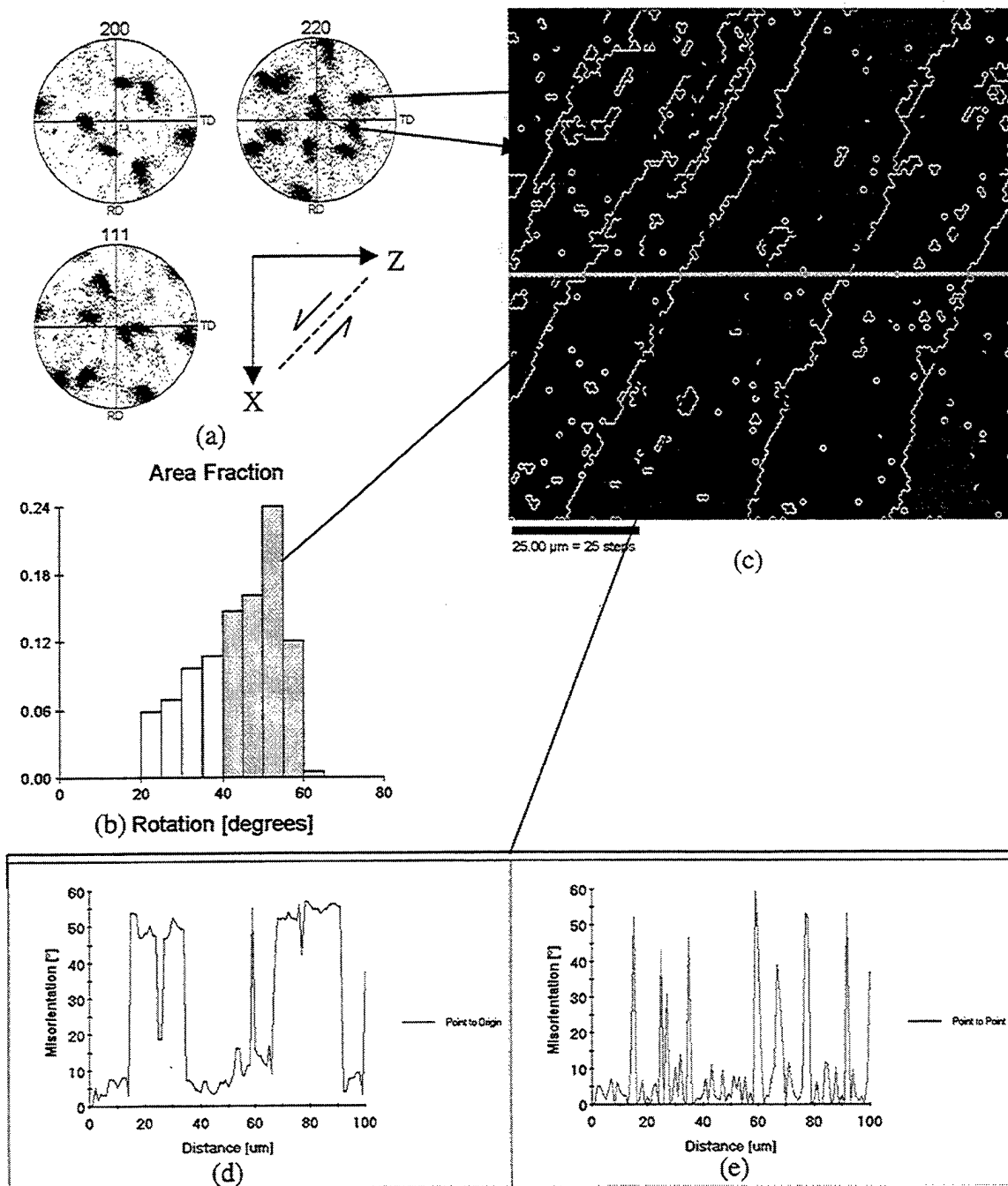
Figure 4.18. OIM Analysis of ECAP aluminum after four pressings by Route B_C. Data are from the center of the Y plane in a 100μm X 100μm region showing the (a) low index pole figures, (b) rotation angle histogram {rotation ≥ 20°}, (c) color coded orientation map with high angle {θ>40°} boundaries highlighted, (d) point to point disorientations and (e) point to origin misorientations from a linear traverse indicated in (c). The point to origin plot demonstrates the evidence of bands of alternating lattice orientation.
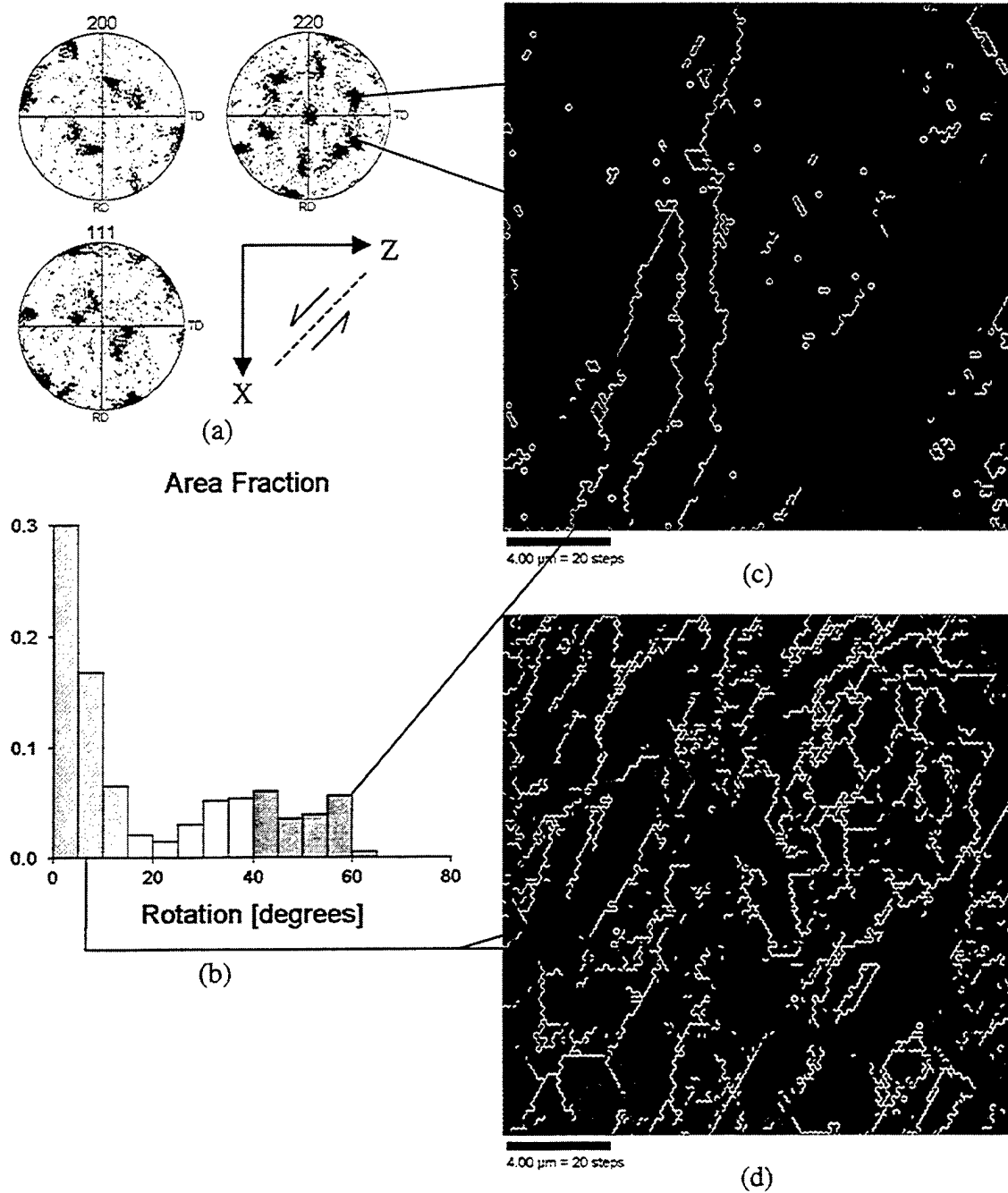
Figure 4.19. OIM Analysis of a 20μm X 20μm area at the center of the Y plane from aluminum after four ECAP pressings by Route B$_C$. Data are showing (a) Pole Figures, (b) Rotation angle Histogram and color coded orientation maps with highlighted (c) high angle {θ>40°} and (d) low angle {2°<θ<15°} boundaries. The large bands are separated by the high angle boundaries and the substructure within each band is separated by low angle boundaries. Both the large bands and substructure tend to align and elongate in the direction of the last shearing.

60
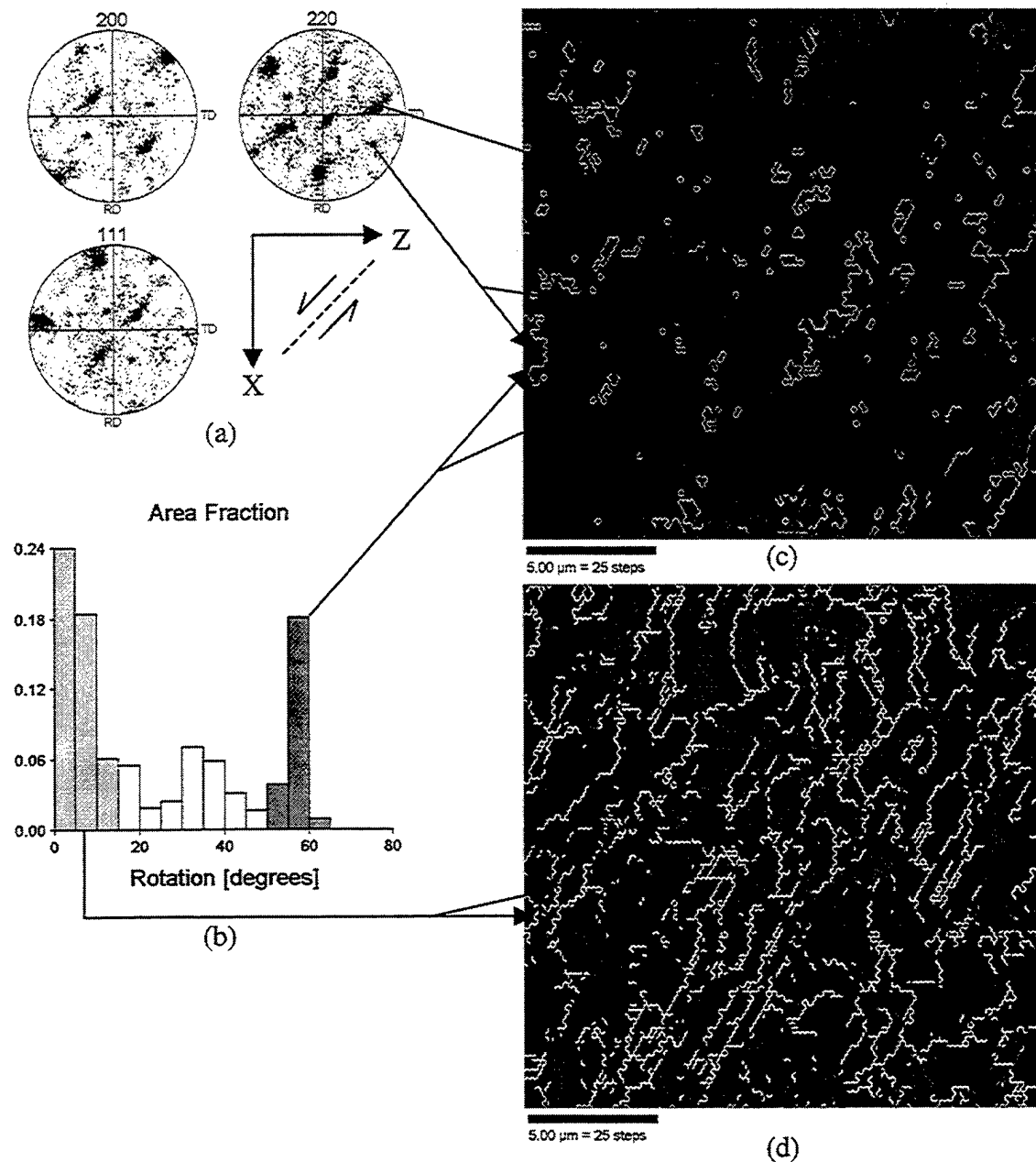
Figure 4.20. OIM analysis of a region near that for the data of Figure 4.19. Here, this 20μm X 20μm region is located almost entirely within one band and hence shows only one major orientation in the (a) pole figure although a second, minor orientation is still evident. In (b), the rotation angle histogram is correlated with the grain boundaries. Grains separated by (c) high angle boundaries and the (d) substructure within the band separated by low angle boundaries.
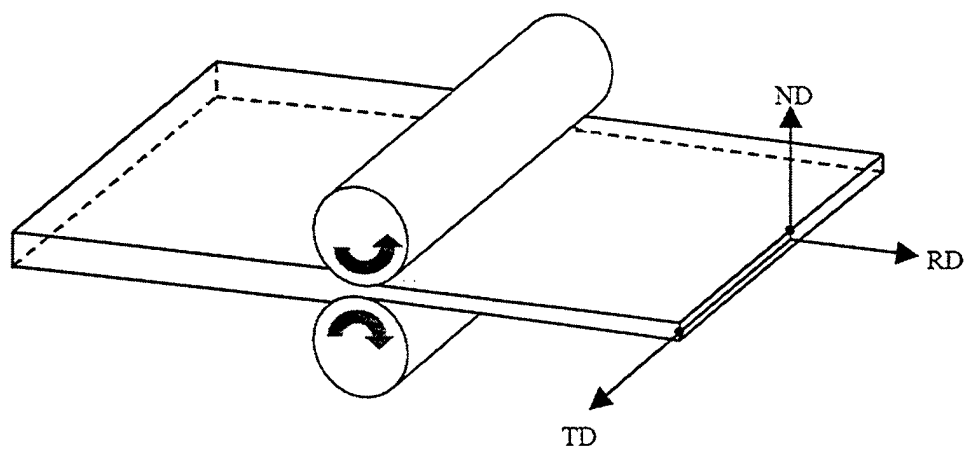
(a)
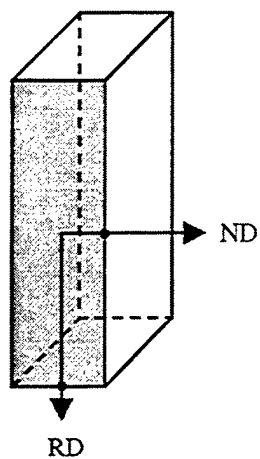
(a)

Figure 4.21. Schematic of a rolled sheet for Supral2004. The axes are indicated as Rolling Direction (RD), Normal Direction (ND) and Transverse Direction (TD). In (b), a schematic shows the sample after sectioning, the shaded surface indicating the plane examined.
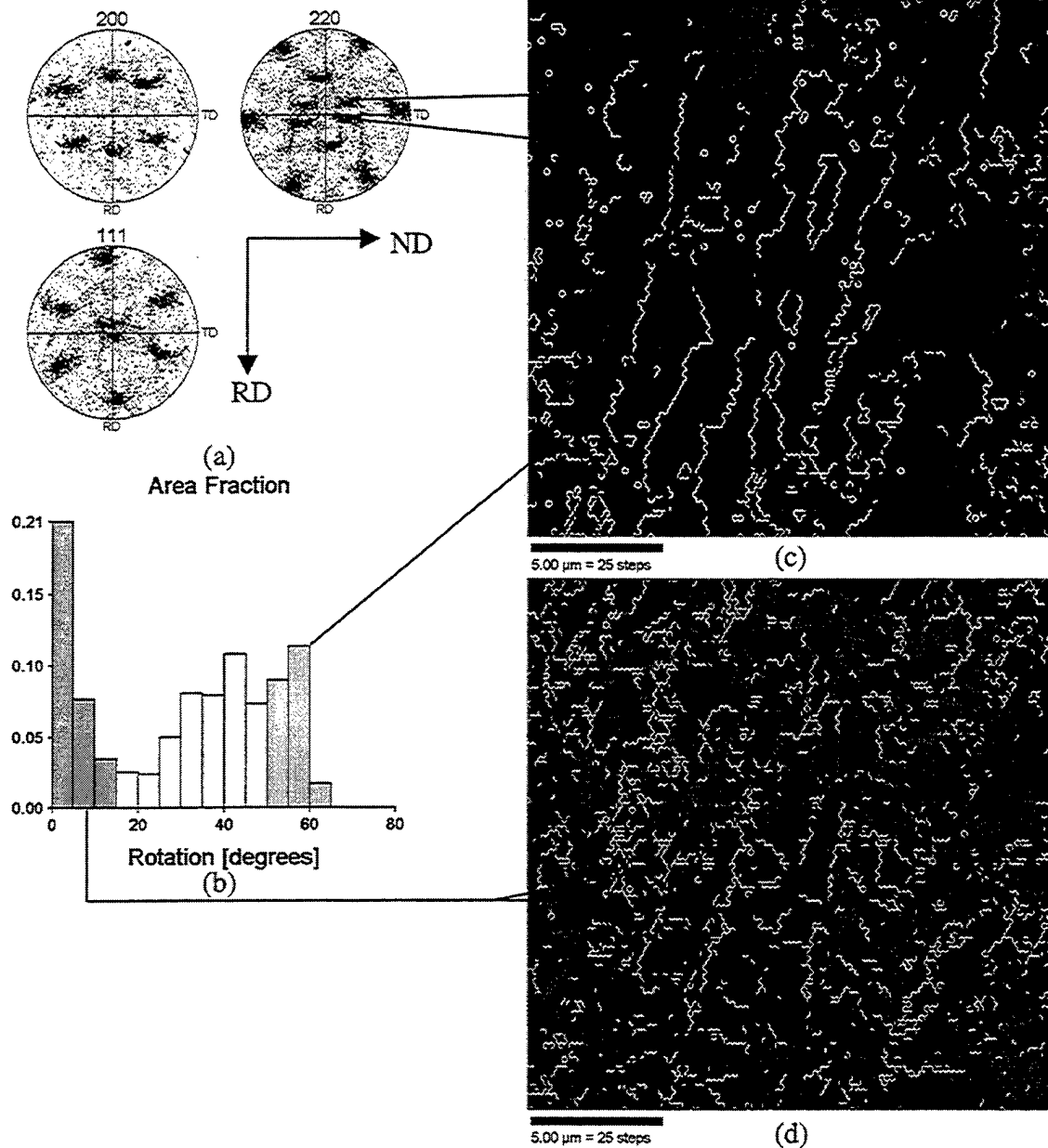
Figure 4.22. OIM Analysis of Supral2004 that has been rolled and annealed. Data are for the Transverse Plane, showing the (a) pole figures, (b) rotation angle histogram and color coded orientation maps with highlighted (c) high angle $\{\theta > 50°\}$ and (d) low angle $\{2° < \theta < 15°\}$ boundaries. When compared to Figures 4.19 and 4.20, a similar structure, consisting of high angle boundaries separating the predominant orientations and a substructure within each band separated by low angle boundaries, becomes apparent. A distinct difference between this figure and Figures 4.19 and 4.20 are the relative sizes of the bands, 2-4μm in width for Supral2004 and 15-25μm for ECAP aluminum.
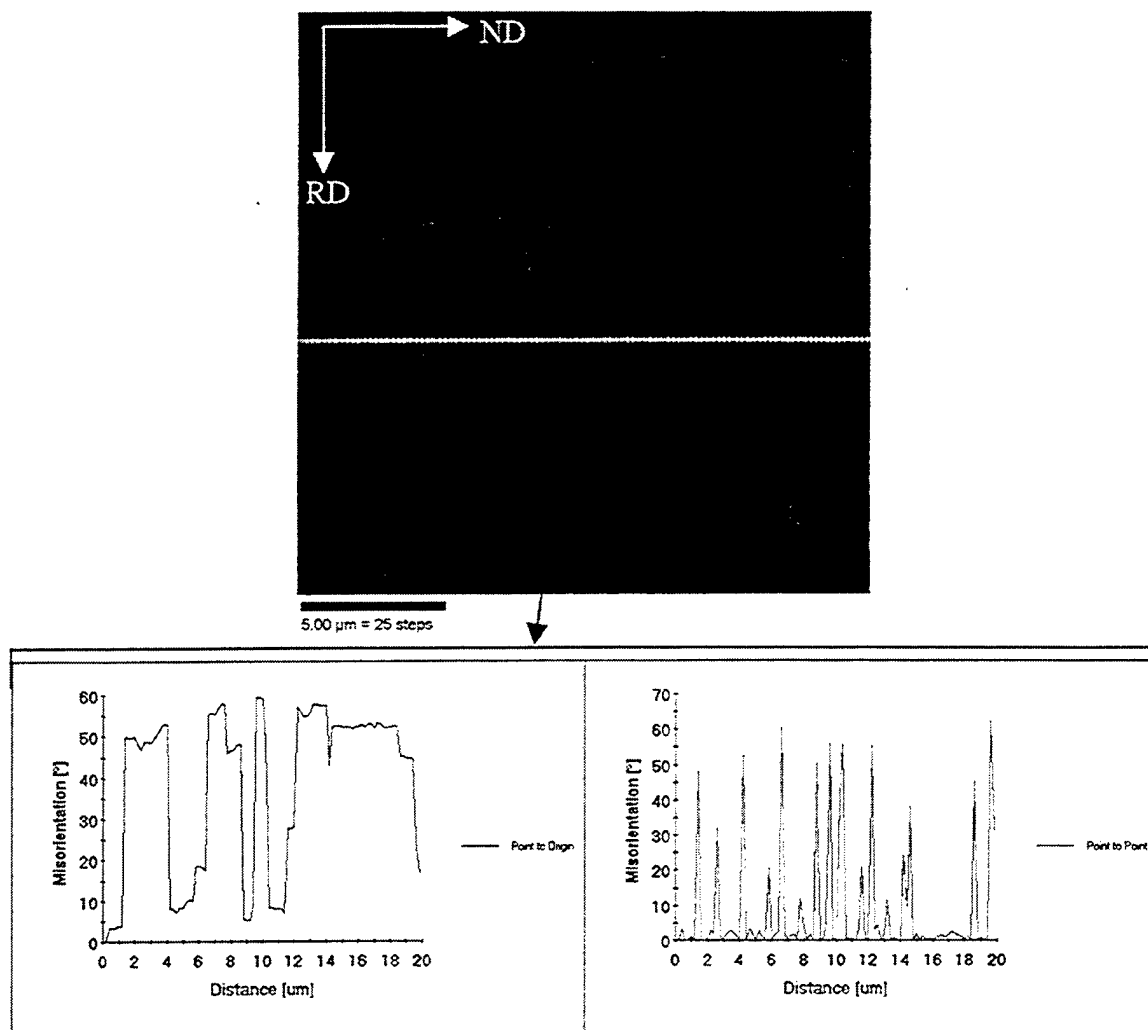
Figure 4.23. Color coded (a) orientation map from the transverse plane of rolled and annealed Supral2004 indicating the position of a linear traverse for obtaining the (b) Point to Origin and (c) Point to Point Misorientation distributions. When compared to Figure 4.18, a similar alternating band structure is apparent. The band interfaces have the same misorientations, as seen in (b), and the band boundaries have characteristic 50-60° Point to Point disorientations, as seen in (c).

V.   SUMMARY AND CONCLUSIONS

A.   SUMMARY AND CONCLUSIONS

The following general conclusions can be drawn from the study of ECAP of 99.99% pure aluminum.

(1) After one ECAP pass, the microstructure is both inhomogeneous and anisotropic.

(2) After repetitive ECAP, the grain size becomes homogeneous but anisotropic character in the microstructure is still evident.

(3) There is a general decrease in the fraction of low angle ($\theta<15°$) as the number of pressing operations increase and there is a corresponding increase in the fraction of high angle ($\theta>15°$) grain boundaries.

(4) Even after 12 ECAP passes the microstructure includes a significant fraction of deformation-induced boundaries.

(5) Deformation banding was observed in both ECAP material and Supral 2004; this phenomenon may contribute significantly to the evolution of the microstructure and may account for the many of the high-angle boundaries produced by deformation processing.

B. RECOMMENDATIONS FOR FUTHER STUDY

The principal recommendation is that further study of deformation banding and its role in microstructural evolution be carried out. Investigations should include the origin and nature of both the high- and low-angle grain boundaries; consideration in the study of other elements and alloy systems; and the incorporation of other plastic deformation techniques. Deformation banding still remains to be explained in detail and a model based on first principle considerations is required. Research in this area may also aid in creation of a predictive model for grain refinement by severe plastic deformation.

LIST OF REFERENCES

1. Bijvoet, J.M., Burgers, W.G., and Hagg, G., "Early Papers on Diffraction of X-Rays," published for the *International Union of Crystallography*, N.V.A. Osstoek's Uitgeversmaatschappij, Utrecht, The Netherlands, 1969.

2. Suryanarayana, C. and Grant Norton, M., *X-Ray Diffraction A Practical Approach*, Plenum Press, 1998.

3. Smallman, R.E., *Modern Physical Metallurgy*, 4th ed., Butterworths, 1985.

4. Hall, E.O., *Proc. Phys. Soc. B*, v. 64, p. 747, 1951.

5. Petch, N.J., *JISI*, v. 173, p. 25, 1953.

6. Doherty, R.D., Hughes, D.A., Humphreys, F.J., Jonas, J.J., Juul Jensen, D., Kassner, M.E., King, W.E., McNelley, T.R., McQueen, H.J., and Rollett, A.D., "Current Issues in Recrystallization: A Review," *Mater. Sci. Engng.*, v. A238, p. 219-274, 1997.

7. Doherty, R.D., Gottstein, G., Hirsch, J.R., Huttchinson, W.B., Lucke, K., Nes, E., and Wilbrandt, P.J., *Panel Discussion on Recrystallization Texture*, ICO-TOM 8, Warrendale, PA, p. 369, 1988.

8. Haasen, P., *Metall. Trans.*, v. 24A, p. 1001, 1993.

9. Gleiter, H., "Materials with Ultrafine Microstructures: Retrospectives and Perspectives," *NanoStructured Materials*, v. 1, p. 1-19, 1992.

10. Provenzano, V., Louat, N.P., Imam, M.A., and Sadananda, K., "Ultrafine Superstrength Materials," *NanoStructured Materials*, v. 1, p. 89-94, 1992.

11. Valiev, R.Z., Mulyukov, R.R., Ovchinnikov, V.V., and Shabashov, V.A., *Scripta Metall. Mater.*, v. 25, p. 2717, 1991.

12. Akhmadeev, N.A., Kopylov, V.I., Mulyoukov, R.R., and Valiev, R.Z., *Iav. Akad. Nauk SSSR Met.*, v. 5, p. 96, 1992.

13. Wang, J., Horita, Z., Furukawa, M., Nemoto, M., Tsenev, N.K., Valiev, R.Z., Ma, Y., and Langdon, T.G., *J. Mater. Res.*, v. 8, p. 2810, 1993.

14. Iwahashi, Y., Horita, Z., Nemoto, M., and Langdon, T.G., *Acta Mater.*, v. 46, p. 3317, 1998.

15. Wang, J., Horita, Z., Furukawa, M., Nemoto, M., Valiev, R.Z., and Langdon, T.G., *Mater. Sci. Engng.*, v. A216, p. 41, 1996.

16. Berbon, P., Furukawa, M., Horita, Z., Nemoto, M., Tsenev, N., Valiev, R.Z., and Langdon, T.G., "An Investigation of the Properties of an Al-Mg-Li-Zr Alloy After Equal-Channel Angular Pressing," *Mater. Sci. Forum*, v. 217-222, p. 1013-1018, 1996.

17. Iwahashi, Y., Horita, Z., Nemoto, M., and Langdon, T.G., "An Investigation of Microstructural Evolution During Equal-Channel Angular Pressing," *Acta Mater.*, v. 45, p. 4733-4741, 1997.

18. Furukawa, M., Iwahashi, Y., Horita, Z., Nemoto, M., and Langdon, T.G., "The Shearing Characteristics Associated with Equal-Channel Angular Pressing," *Mater. Sci. Engng.*, v. A257, p. 328-332, 1998.

19. Horita, Z., Furukawa, M., Oh-ishi, K., Nemoto, M., and Langdon, T.G., "Equal-Channel Angular Pressing for Grain Refinement of Metallic Materials," published for *The Fourth International Conference on Recrystallization and Related Phenomena*, The Japan Institute of Metals, 1999.

20. Iwahashi, Y., Wang, J., Horita, Z., Nemoto, M., and Langdon, T.G., *Scripta Mater.*, v. 35, p. 143, 1996.

21. Furukawa, M., Iwahashi, Y., Horita, Z., Nemoto, M., and Langdon, T.G., *Metall. Mater. Trans.*, v. 29A, p. 2245, 1998.

22. Oh-ishi, K., Furukawa, M., Horita, Z., Nemoto, M., and Langdon, T.G., *Metall. Mater. Trans.*, v. 29A, p. 2011, 1998.

23. Nakashima, K., Horita, Z., Nemoto, M., and Langdon, T.G., *Acta Mater.*, v. 46, p. 1589, 1998.

24. Iwahashi, Y., Horita, Z., Nemoto, M., and Langdon, T.G., *Metall. Mater. Trans.*, v. 29A, p. 2503, 1998.

25. Randle, V., *Microtexture Determination and Its Applications*, The Institute of Materials, 1992.

26. Read, W.T. Jr., *Dislocations in Crystals*, McGraw-Hill, 1953.

27. Bunge, H.J., *Texture Analysis in Materials Science*, Butterworths, 1982.

28. Barrett, C.S., *Trans. Am. Inst. Min. Engrs.*, v. 135, p. 296, 1939.

29. Barrett, C.S. and Levenson, L.H., *Trans. Am. Inst. Min. Engrs.*, v. 137, p. 112-127, 1940.

30. Lee, C.S., Duggan, B.J., and Smallman, R.E., *Acta Metall. Mater.*, v. 41, p. 2265, 1993.

31. Lee, C.S. and Duggan, B.J., *Acta Metall. Mater.*, v. 41, p. 2691, 1993.

32. Lee, C.S., Duggan, B.J., and Smallman, R.E., *J. Phys. IV*, v. C7, p. 2027, 1993.

33. Lee, C.S., Smallman, R.E., and Duggan, B.J., *Scripta Metall. Mater.*, v. 33, p. 72, 1995.

34. Kulkarni, K., Starke, E.A. Jr., Kuhlmann-Wilsdorf, D., *Acta Mater.*, v. 46, p. 5283, 1998.

35. Hirsch, J. and Lücke, K., *Acta Metall.*, v. 36, p. 2863, 1988.

36. McNelley, T.R., McMahon, M.E., and Pérez-Prado, M.T., *Phil. Trans. Roy. Soc. A*, v. 357, p. 1683, 1999.

THIS PAGE INTENTIONALLY LEFT BLANK

INITIAL DISTRIBUTION LIST

1. Defense Technical Information Center 2
    8725 John J. Kingman Road, Suite 0944
    Ft. Belvoir, VA 22060-6218

2. Dudley Knox Library 2
    Naval Postgraduate School
    411 Dyer Road
    Monterey, CA 93943-5101

3. Engineering and Technology Curricular Office, Code 34 1
    Naval Postgraduate School
    700 Dyer Road, Bldg. 245
    Monterey, California 93943-5100

4. Department Chairman, Code ME/Mc 1
    Naval Postgraduate School
    700 Dyer Road, Bldg. 245
    Monterey, California 93943-5100

5. Professor Terry R. McNelley, Code ME/Mc 4
    Naval Postgraduate School
    700 Dyer Road, Bldg. 245
    Monterey, California 93943-5100

6. LT Douglas L. Swisher 2
    211 Normandy Road
    Seaside, California 93955

7. Professor Terrence G. Langdon.. 1
    Departments of Aerospace & Mechanical Engineering and Materials Science
    University of Southern California
    Los Angeles, California 90089-1453

8. Professor Zenji Horita 1
    Department of Materials Science and Engineering, Faculty of Engineering 36
    Kyushu University
    Fukuoka 812-81 Japan

9. Dr. M.Teresa Pérez-Prado 1
    Centro Nacional de Investigaciones Metalurgicas
    Avda. Gregorio del Amo
    8-28040 Madrid, Spain